

Black shale deposition, atmospheric CO₂ drawdown, and cooling during the Cenomanian-Turonian Oceanic Anoxic Event

Ian Jarvis,¹ John S. Lignum,^{1,2} Darren R. Gröcke,³ Hugh C. Jenkyns,⁴ and Martin A. Pearce⁵

Received 19 November 2010; revised 22 February 2011; accepted 13 April 2011; published 19 July 2011.

[1] Oceanic Anoxic Event 2 (OAE2), spanning the Cenomanian-Turonian boundary (CTB), represents one of the largest perturbations in the global carbon cycle in the last 100 Myr. The $\delta^{13}\text{C}_{\text{carb}}$, $\delta^{13}\text{C}_{\text{org}}$, and $\delta^{18}\text{O}$ chemostratigraphy of a black shale-bearing CTB succession in the Vocontian Basin of France is described and correlated at high resolution to the European CTB reference section at Eastbourne, England, and to successions in Germany, the equatorial and midlatitude proto-North Atlantic, and the U.S. Western Interior Seaway (WIS). $\Delta^{13}\text{C}$ (offset between $\delta^{13}\text{C}_{\text{carb}}$ and $\delta^{13}\text{C}_{\text{org}}$) is shown to be a good $p\text{CO}_2$ proxy that is consistent with $p\text{CO}_2$ records obtained using biomarker $\delta^{13}\text{C}$ data from Atlantic black shales and leaf stomata data from WIS sections. Boreal chalk $\delta^{18}\text{O}$ records show sea surface temperature (SST) changes that closely follow the $\Delta^{13}\text{C}$ $p\text{CO}_2$ proxy and confirm TEX₈₆ results from deep ocean sites. Rising $p\text{CO}_2$ and SST during the Late Cenomanian is attributed to volcanic degassing; $p\text{CO}_2$ and SST maxima occurred at the onset of black shale deposition, followed by falling $p\text{CO}_2$ and cooling due to carbon sequestration by marine organic productivity and preservation, and increased silicate weathering. A marked $p\text{CO}_2$ minimum (~25% fall) occurred with a SST minimum (Plenus Cold Event) showing >4°C of cooling in ~40 kyr. Renewed increases in $p\text{CO}_2$, SST, and $\delta^{13}\text{C}$ during latest Cenomanian black shale deposition suggest that a continuing volcanogenic CO₂ flux overrode further drawdown effects. Maximum $p\text{CO}_2$ and SST followed the end of OAE2, associated with a falling nutrient supply during the Early Turonian eustatic highstand.

Citation: Jarvis, I., J. S. Lignum, D. R. Gröcke, H. C. Jenkyns, and M. A. Pearce (2011), Black shale deposition, atmospheric CO₂ drawdown, and cooling during the Cenomanian-Turonian Oceanic Anoxic Event, *Paleoceanography*, 26, PA3201, doi:10.1029/2010PA002081.

1. Introduction

[2] The mid-Cretaceous, Aptian to earliest Turonian time (125–93 Ma), was characterized by high rates of seafloor spreading and multiple pulses of extensive volcanic activity [Arthur *et al.*, 1985b; Larson, 1991; Seton *et al.*, 2009]. Volcanic out-gassing led to high atmospheric CO₂ concentrations of up to 3–5 times preindustrial levels [Bernier, 2006; Fletcher *et al.*, 2008; Barclay *et al.*, 2010]. Climate proxy data indicate a period of optimum global warmth, high sea surface temperatures (SST), and a much reduced equator-to-pole thermal gradient [Barron, 1983; Huber *et al.*, 1995, 2002; Bice *et al.*, 2006; Forster *et al.*, 2007;

Sinninghe Damsté *et al.*, 2010]. High $p\text{CO}_2$ (partial pressure CO₂) and warm climates increased terrestrial weathering and input of fluvial nutrient fluxes, and decreased the levels of oxygen in the atmosphere and oceans.

[3] Episodes of widespread black shale deposition are a characteristic feature of the mid-Cretaceous sedimentary record and have been termed Oceanic Anoxic Events (OAEs) [Schlanger and Jenkyns, 1976; Arthur *et al.*, 1987; Schlanger *et al.*, 1987], but the causes of these phenomena remain hotly debated. It is likely that increased nutrient availability and intensified upwelling, particularly where associated with restricted basin geometries, generally poor oceanic oxygenation, weakened circulation and possible density stratification, made the mid-Cretaceous oceans predisposed to periods of bottom water anoxia and local euxinic (sulfidic) conditions, thus enhancing the preservation of organic matter (e.g., see discussion by Jenkyns [2010]).

[4] Once established, euxinic conditions allowed phosphate release back to bottom waters from degrading organic matter, establishing a positive feedback loop that maintained productivity, euxinia and carbon burial until the original

¹Centre for Earth and Environmental Science Research, School of Geography, Geology and the Environment, Kingston University London, Kingston upon Thames, UK.

²Ichron Limited, Northwich, UK.

³Department of Earth Sciences, Durham University, Durham, UK.

⁴Department of Earth Sciences, University of Oxford, Oxford, UK.

⁵Statoil Gulf Services LLC, Houston, Texas, USA.

forcing was removed [Mort et al., 2007; Meyer and Kump, 2008; Tsandev and Slomp, 2009]. Additionally, release of trace-metal micronutrients [Snow et al., 2005] and sulfur associated with massive volcanism [Turgeon and Creaser, 2008] may have further enhanced productivity and facilitated carbon remineralization and enhanced nutrient recycling, which increased the already high levels of global primary production [Adams et al., 2010].

[5] In addition to black shale deposition, OAEs are “classically” marked by the global development of short-lived (<1 Myr) positive carbon stable-isotope ($\delta^{13}\text{C}$) excursions in marine carbonates, and both marine and nonmarine organic matter [Scholle and Arthur, 1980; Schlanger et al., 1987; Arthur et al., 1988; Hasegawa, 1997; Tsikos et al., 2004; Jarvis et al., 2006; Jenkyns, 2010], caused by the enhanced burial of ^{13}C -depleted organic matter. OAEs thus represent dramatic short-term perturbations of the global carbon cycle.

[6] The last major mid-Cretaceous anoxic event, referred to as Oceanic Anoxic Event 2 (OAE2) [e.g., Jenkyns, 2010], and one of few with a truly global distribution, occurred across the Cenomanian-Turonian boundary (CTB) at 93.6 Ma [Ogg et al., 2008], and lasted for approximately 500 kyr [Sageman et al., 2006; Voigt et al., 2008]. It has been argued that high burial rates of organic carbon during the CTB event were sufficient to significantly draw down atmospheric CO₂ and cause transient cooling of the global climate [Arthur et al., 1988; Freeman and Hayes, 1992; Kuypers et al., 1999]. Recent studies of ocean drilling cores [Forster et al., 2007; Sinninghe Damsté et al., 2008, 2010] support this hypothesis. However, the stratigraphic and temporal resolution offered by deep-sea cores is poor, typically consisting of thin, commonly incomplete CTB successions of black shale with sparse and poorly preserved biota containing few biostratigraphic index species; making it difficult to precisely place the paleoenvironmental changes accompanying OAE2.

[7] In this paper, an expanded onshore CTB succession with black shales is described from Pont d’Issole in the Vocontian Basin of SE France. The section yields abundant nannofossils, planktonic foraminifera, and organic-walled dinoflagellate cysts which, together with paired carbonate-carbon ($\delta^{13}\text{C}_{\text{carb}}$) and organic-carbon ($\delta^{13}\text{C}_{\text{org}}$) stable-isotope records, allow bed-scale correlation with the European CTB reference section at Eastbourne, England [Paul et al., 1999; Tsikos et al., 2004; Gale et al., 2005; Pearce et al., 2009], and other sections worldwide. Carbon and oxygen stable-isotope records at Pont d’Issole, supported by marine biomarker and fossil leaf (stomata count) $p\text{CO}_2$ paleoproxy and biomarker (TEX₈₆) paleotemperature data from correlative terrestrial and oceanic sites, provide strong evidence for major short-term variation in atmospheric CO₂ tied to varying organic carbon burial and silicate weathering rates that ultimately drove changes in SST.

2. Geological Setting

[8] During Cenomanian-Turonian time, the Vocontian Basin was a western gulf in the European Alpine realm of the northern Tethys Ocean, located at approximately 30°N (Figure 1). Subsidence in the deeper central and eastern parts of the basin provided accommodation for thick,

cyclically bedded, bioturbated limestone-marl hemipelagic successions that now form marl-dominated slopes at outcrop for the Cenomanian and prominent limestone cliffs for the Turonian. Paleowater depths were likely in the order of a few hundred meters in the central basin [Wilpshaar et al., 1997; Grosheny et al., 2006], with evidence of storm-influenced deposition on the adjacent outer platform.

[9] A marked facies change occurs through the CTB interval in the deeper basin, with the occurrence of a distinctive, up to 20 m thick, package of dark marls containing beds of black calcareous shales, termed the Niveau Thomel [Crumière, 1989]. These organic-rich beds are one of the best developed on-land expressions of OAE2. By contrast, black shale facies are unknown on the margins of the Vocontian Basin, and are only a few centimeters thick in the central basin; they expand substantially in the eastern domain, toward the connection to the open Tethys Ocean.

3. Material and Methods

[10] Results of an integrated lithostratigraphic, biostratigraphic and chemostratigraphic study of a Vocontian Basin CTB reference section at Pont d’Issole are presented here. The section was chosen in preference to the better known outcrop at Vergons [Crumière, 1989; Crumière et al., 1990] because the CTB boundary interval is thicker and more complete at Pont d’Issole [Morel, 1998; Grosheny et al., 2006; Lignum, 2009]; synsedimentary slumping and/or later faulting have removed the lower black shale beds of the Niveau Thomel at Vergons.

[11] Samples of ~1 kg were collected at approximately 50 cm intervals through the 25 m thick section exposed at Pont d’Issole (44.0699°N 6.4828°E, 1064 m altitude), 500 m SE of the village of La Bâtie Thorame-Basse, Alpe de Haute Provence. The succession displays two prominent black shale intervals within an interbedded limestone–gray marl succession (Figure 2). Crumière [1991], Morel [1998], and Grosheny et al. [2006] presented selected foraminifera and calcareous nannofossil biostratigraphic data for the Pont d’Issole section.

[12] Analysis of the organic-walled dinoflagellate cyst (dinocyst) assemblages in the samples was undertaken by Lignum [2009] using the method of Lignum et al. [2008]. To assess the relative contribution of terrestrial material to the palynomorph assemblage, the terrestrial/marine palynomorph (T/M) index, $I = t/(m + t)$, with t = number of terrestrial palynomorphs (spores and pollen) and m = number of marine palynomorphs (dinocysts and acritarchs), was calculated [Pross, 2001]. The combined foraminiferal, nannofossil and dinocyst data provide a robust biostratigraphic framework for the chemostratigraphic study presented here.

[13] Subsamples (typically 50 g) were washed with tap water and allowed to dry before being crushed to <3 mm chips in clean thick-walled plastic bags, using a metal plate and hammer. The chips were pulverized to a fine powder in a planetary mill with agate vessels and balls. Carbon and oxygen stable-isotope determinations of the carbonate fraction ($\delta^{13}\text{C}_{\text{carb}}$, $\delta^{18}\text{O}$) in powdered samples were made at the University of Oxford following the method of Jenkyns et al. [1994]. Data are reported in standard delta (δ) nota-

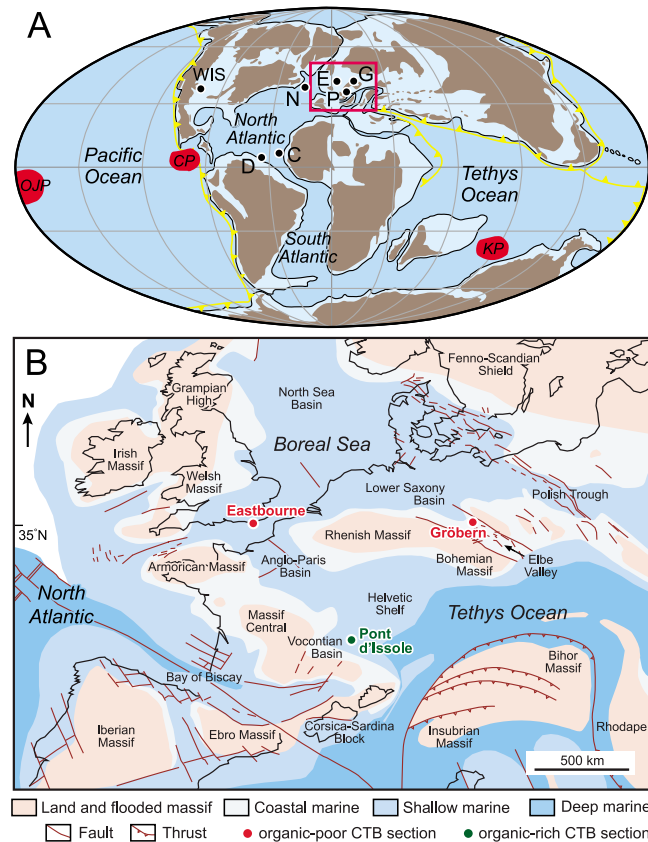


Figure 1. Late Cenomanian paleogeography and location of sites. (a) Global paleogeography at 90 Ma showing position of Cretaceous subduction zones (yellow) and large igneous provinces or LIPs (red): CP, Caribbean Plateau; KP, Kerguelen Plateau; OJP, Ontong-Java Plateau. Cenomanian-Turonian boundary sites: C, Cape Verde Basin; D, Demerara Rise; E, Eastbourne; G, Gröbern; N, Newfoundland Basin; P, Pont d'Issole; WIS, Western Interior Seaway. Reconstruction based on R.C. Blakey, NAU Geology (<http://jan.ucc.nau.edu/~rcb7/90moll.jpg>). (b) Cenomanian paleogeography of Europe showing location of the main study sites. CTB is Cenomanian-Turonian boundary. Modified from Philip *et al.* [2000].

tion as per mil (‰) relative to the Vienna Peedee belemnite (VPDB) standard.

[14] For carbon-isotope determination of the organic fraction ($\delta^{13}\text{C}_{\text{org}}$), 2 g of sample powders were decalcified by addition of 10 mL 10% (1.2 M) HCl, followed by 10 mL 25% (3 M) HCl in an ultrasonic water bath at 60°C. Carbon-isotope measurements were performed on the insoluble residues using a Costech ESC4010 Elemental Analyzer (EA) connected to a ThermoFinnigan Delta V Advantage isotope ratio mass spectrometer (IRMS) via a ConFlo III interface at the University of Durham. Carbon-isotope ratios were Craig-corrected for ^{17}O contribution and are reported relative to the VPDB scale. Up to eight international and internal standards were analyzed continuously throughout the generation of each isotopic data set. Total organic carbon (TOC) data were obtained from the mass area of CO_2 produced in the EA and determined in the IRMS. TOC was calculated using a k-factor generated from an internal standard, glutamic acid (C = 40.82%). Analysis of selected samples by stand-alone EA revealed no significant difference with data obtained by EA-IRMS. Reproducibility of replicate samples was generally better than 0.1‰ for $\delta^{13}\text{C}_{\text{carb}}$, $\delta^{13}\text{C}_{\text{org}}$ and $\delta^{18}\text{O}$, and 0.2 wt% for TOC in the insoluble residue.

[15] For the determination of Ca and Al, dried samples were fused with lithium metaborate (LiBO_2) flux in graphite crucibles in a muffle furnace at 1050°C, and the melts were dissolved in 0.3 M nitric acid (HNO_3), following the method of Jarvis [2003]. Analyses were performed by inductively coupled plasma-atomic emission spectroscopy (ICP-AES) employing a JY Ultima 2C spectrometer at Kingston University London, calibrated using in-house rock reference materials [Lignum, 2009]. CaCO_3 values were calculated from total Ca contents assuming that all Ca resides in the carbonate fraction. By reference to international standard reference materials run with samples, accuracy and precision for Ca and Al were judged to be <3%. Numerical data are presented in the auxiliary materials.¹

4. Stratigraphy

4.1. Lithostratigraphy

[16] The base of the Niveau Thomel at Pont d'Issole is taken at the marked facies change from indurated thick-bedded very pale gray, pale yellow-weathering, bioturbated

¹Auxiliary materials are available in the HTML. doi:10.1029/2010PA002081.

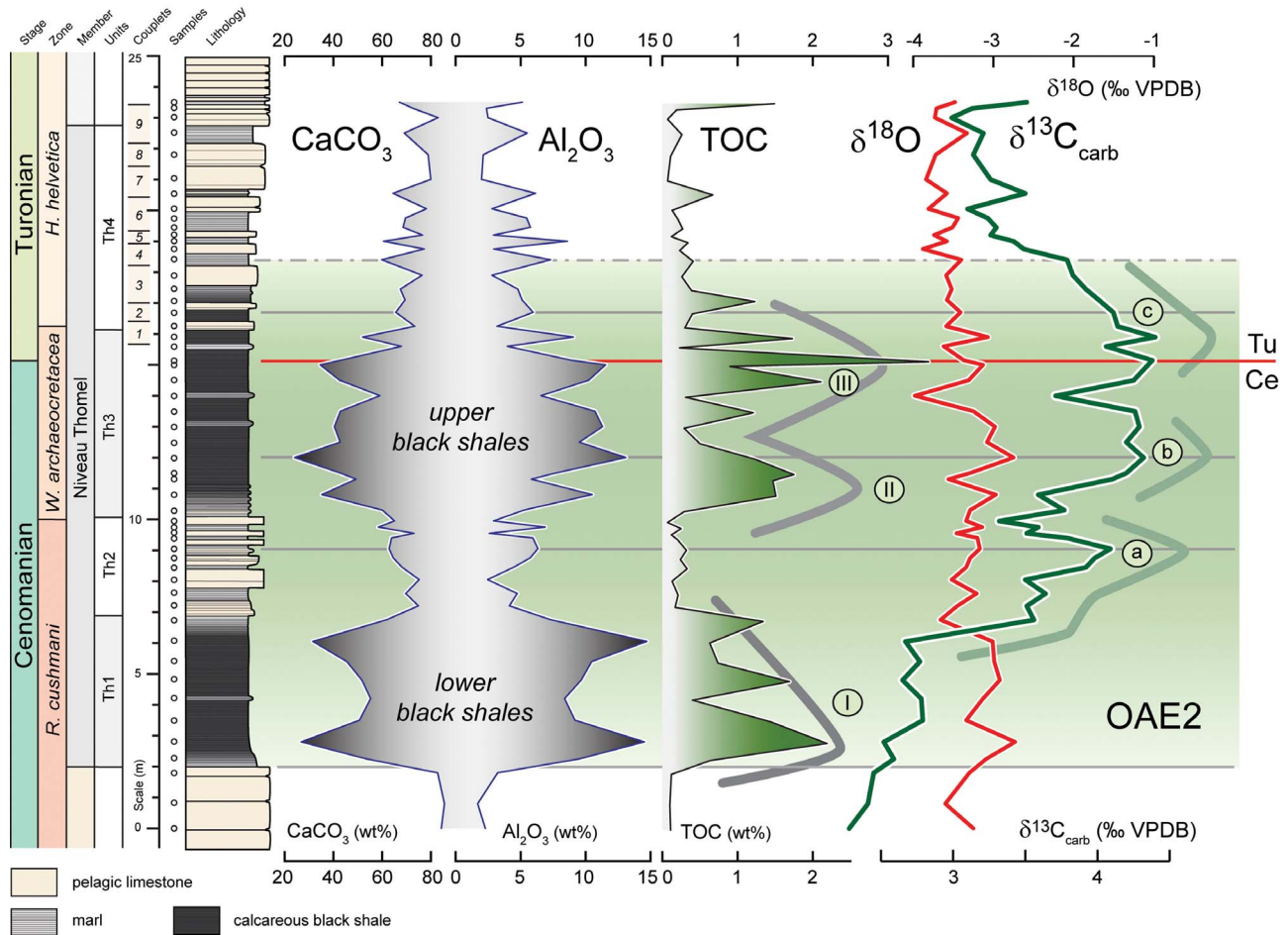


Figure 2. Stratigraphy of the CTB succession at Pont d'Issole. The organic-rich interval of the Niveau Thomel includes two black shale packages separated and overlain by intervals of interbedded limestones and marls. Peaks in total organic carbon (TOC) content (Units I–III) precede the three maxima (a, b, and c) in carbon stable-isotope values of the bulk sediment carbonate fraction ($\delta^{13}\text{C}_{\text{carb}}$). Green shading indicates the interval of the positive $\delta^{13}\text{C}$ excursion defining Oceanic Anoxic Event 2 (OAE2). Thick gray and green curves indicate the interpreted positions of maximum TOC and $\delta^{13}\text{C}$ peaks, respectively.

limestones, to friable black laminated shales and weakly bioturbated dark gray marls (Figure 2). The top of the Niveau Thomel is placed at the top of the last thick marl bed. Samples display significant lithological variation within the black shale intervals, but details at outcrop were obscured by poor exposure of these beds.

[17] The limestones at the base of the section (Figure 2) are bioturbated nanofossil-foraminiferal wackestones containing abundant and diverse planktonic foraminifera assemblages, including common large keeled morphotypes, particularly rotaliporids, with common benthic foraminifera, radiolaria and sponge spicules. The Niveau Thomel comprises four lithological units (Th1–4, Figure 2): laminated black shales with weakly bioturbated (dominantly *Chondrites*) dark gray marls (units Th1 and Th3); and interbedded bioturbated gray marls and limestones (units Th2 and Th4). Laminated beds are calcareous mudstones with millimetric alternations of amorphous organic matter-rich and more detritus-rich (clay minerals and fine silt-sized quartz) lamellae. Spar-filled molds of radiolaria are common, but planktonic foraminifera

are small and rare, and benthic foraminifera are absent. Weakly bioturbated beds contain more dispersed organic matter, with phosphate and glauconite grains and foraminifera tests being more common.

[18] The interbedded limestones and marls (bioturbated wackestones) of units Th2 and Th4 are rich in small planktonic foraminifera and radiolaria, and yield benthic foraminifera and sponge spicules. Unit Th4 shows a very distinct succession of nine marl-limestone couplets (1–9 in Figure 2) which can be correlated on a regional scale. The limestone beds immediately below the Niveau Thomel can also be correlated laterally, but Units Th1–3 show substantial local bedding and thickness variation and are generally thicker at Pont d'Issole than elsewhere in the basin [e.g., Morel, 1998, Figure II.12; Grosheny et al., 2006].

4.2. Biostratigraphy

[19] The age of the succession is constrained by the last appearance of rotaliporids (top Upper Cenomanian *Rotalipora cushmani* zone) at the top of Unit Th2, and the

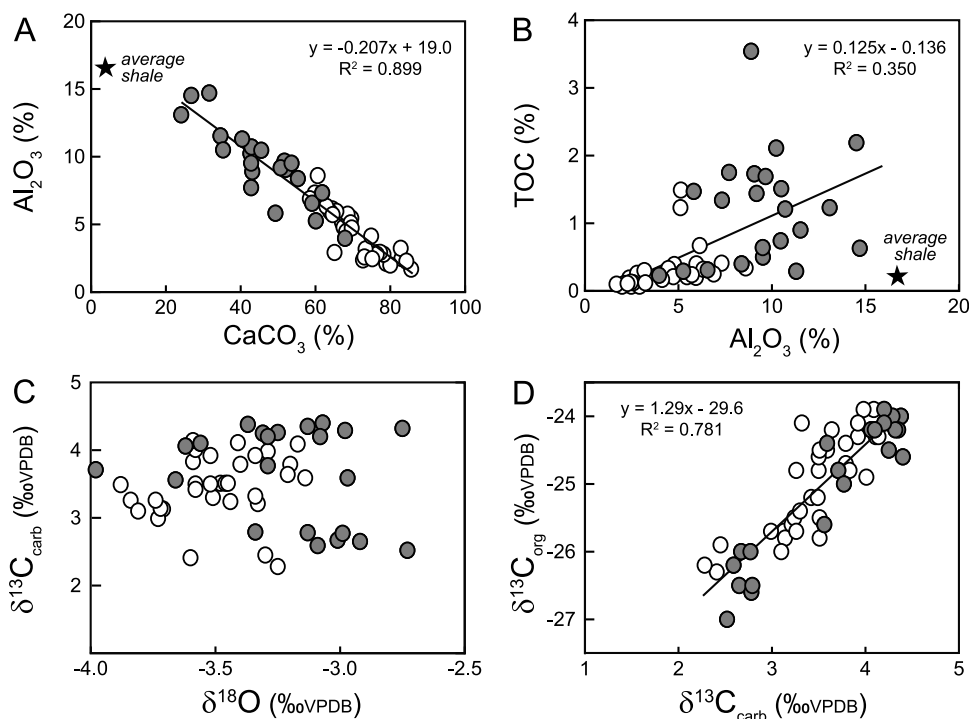


Figure 3. Geochemical crossplots for Pont d'Issole data. (a) Al_2O_3 versus CaCO_3 : the strong negative correlation exemplifies the diluent effect of carbonate on other major constituents, in this case aluminum, a good clay-mineral proxy. Gray filled circles are Niveau Thomel black shale samples; open circles are chalks and marls. The composition of average shale [Wedepohl, 1971] is shown for comparison. (b) Total organic carbon (TOC) versus Al_2O_3 : a weak positive correlation shows that organic matter contents are only moderately affected by carbonate content. Black shale samples have up to one order of magnitude higher TOC contents than average shale (0.2%). (c) Carbon ($\delta^{13}\text{C}_{\text{carb}}$) versus oxygen ($\delta^{18}\text{O}$) isotopes in the carbonate fraction; the absence of any clear trends suggests that diagenetic overprint is minimal. (d) A strong positive correlation between carbon stable isotopes in the carbonate and organic matter ($\delta^{13}\text{C}_{\text{org}}$) fractions supports the retention of a primary paleoenvironmental signal in both components.

first appearance of *Helvetoglobotruncana helvetica* at the bottom of Unit Th4 (Lower Turonian *H. helvetica* zone; Figure 2). The CTB is placed toward the top of the intervening *Whiteinella archaeocretacea* zone in Unit Th3, based on correlation of the carbon stable-isotope profile with the European reference section at Eastbourne, England (section 4.4), where the stage boundary is well constrained by inoceramid bivalves and ammonites [Gale et al., 2005].

4.3. Chemostratigraphy

[20] The main lithological trends through the boundary interval can be quantified from bulk geochemical profiles using Ca, Al and TOC as proxies for carbonate, clays and organic matter, respectively (Figure 2). The Al_2O_3 profile is a near-mirror image of the carbonate (CaCO_3) profile; least squares regression analysis yields a strong negative correlation between the two constituents (Figure 3a). This demonstrates that variations in bulk sediment composition are dominated throughout the section by carbonate (low-Mg calcite) and clay contents, with quartz, glauconite, phosphate, organic matter and other constituents only having a minor influence.

[21] The TOC profile shows three peaks: one at the base of lower black shale Unit Th1 (I in Figure 2), and two in the

lower and upper parts of upper black shale Unit Th3 (II and III, Figure 2). TOC contents are generally highest (maximum 3.5 wt%) in clay-rich beds from the black shale intervals which average 1.2 wt% TOC (Figures 2 and 3), but there is only a weak positive correlation between TOC and Al (Figure 3b).

[22] The carbon-isotope profile for the carbonate fraction ($\delta^{13}\text{C}_{\text{carb}}$) also displays three maxima (a–c, Figure 2) superimposed on the long-term large positive CTB excursion, and these maxima occur immediately above corresponding peaks in TOC. Oxygen isotopes ($\delta^{18}\text{O}$) display an erratic long-term fall up-section. The absence of any correlation between $\delta^{13}\text{C}_{\text{carb}}$ and $\delta^{18}\text{O}$ (Figures 2 and 3c) shows that despite the moderate burial diagenesis indicated by low $\delta^{18}\text{O}$ values of -2.8 to -4.0 ‰, there is no evidence for significant alteration of primary $\delta^{13}\text{C}_{\text{carb}}$ values, which are similar to many other CTB boundary sections worldwide [e.g., Tsikos et al., 2004; Jarvis et al., 2006].

[23] The new isotope data provide higher resolution than a previously published carbon-isotope curve for Pont d'Issole [Morel, 1998; Grosheny et al., 2006]. Very similar chemostratigraphic profiles and values for $\delta^{13}\text{C}_{\text{carb}}$, $\delta^{18}\text{O}$, CaCO_3 and TOC have been documented recently for a CTB section at Lambrouisse [Takashima et al., 2009],

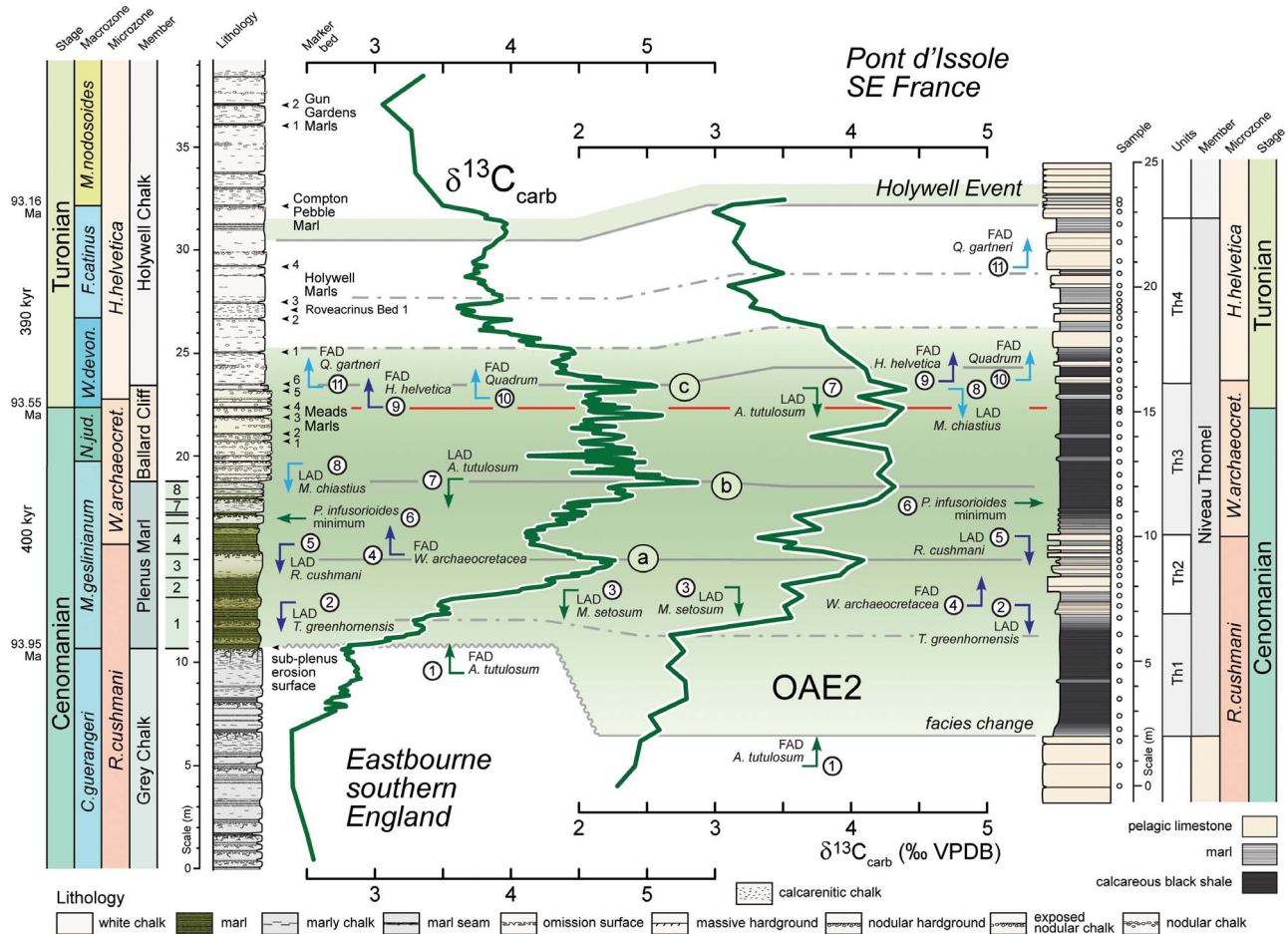


Figure 4. Stratigraphy and $\delta^{13}\text{C}_{\text{carb}}$ curve of the European CTB reference section at Eastbourne correlated to Pont d'Issole. Key biostratigraphic datum levels, numbered 1–11 based on their relative stratigraphic positions at Eastbourne, include first appearances (FAD) and last appearances (LAD) of key planktonic foraminifera (dark blue), calcareous nannofossil (pale blue) and organic-walled dinoflagellate cyst (green) taxa. Gray horizontal lines are key tie points for the isotope correlation; a, b, and c are the three main $\delta^{13}\text{C}$ maxima and inflection points on the broad positive isotope excursion defining the CTB event and OAE2. Eastbourne data are from Pearce *et al.* [2009]; Pont d'Issole biostratigraphic datum levels are compiled from Morel [1998], Grosheny *et al.* [2006], and Lignum [2009]. Age assignments based on orbitally tuned time scale of Voigt *et al.* [2008].

located 4 km to the south of Pont d'Issole, but the lower black shale interval at Pont d'Issole (Th1) is double the thickness of equivalent beds at Lambruisse.

4.4. Chemostratigraphic Correlation

[24] Comparison of the $\delta^{13}\text{C}_{\text{carb}}$ profile at Pont d'Issole with a high-resolution curve from the European CTB boundary reference section at Eastbourne, England [Paul *et al.*, 1999; Pearce *et al.*, 2009] reveals a remarkable similarity in the shapes of the two curves, with slightly higher amplitude fluctuations at Eastbourne (Figure 4), and a marginally thicker sequence at Pont d'Issole. Correlation may be achieved using key peaks and inflection points on the carbon-isotope curves, including peaks a–c of Jarvis *et al.* [2006].

[25] The chemostratigraphic correlation may be tested using 11 common biostratigraphic datum levels, including the first and last appearances of organic-walled dinoflagel-

late cysts (dinocysts), planktonic foraminifera, and calcareous nannofossils (Figure 4). The positions of these datum levels are consistent in the two sections and with the chemostratigraphic correlation. Minor differences are attributed to preservation factors associated with facies changes and difficulties in precisely placing the datum levels of less common species. The correlation enables the positions of the international ammonite biozones determined at Eastbourne to be placed in the SE France succession.

5. Organic Matter

5.1. Characteristics and Origin

[26] The black shale intervals in the Niveau Thomel at Pont d'Issole display TOC contents of 0.3–3.5 wt% (average 1.2 wt%), compared to associated limestone intervals containing <0.3 wt% TOC (Figures 2 and 3b); such values are typical for the area [Crumière, 1989, 1991; Crumière

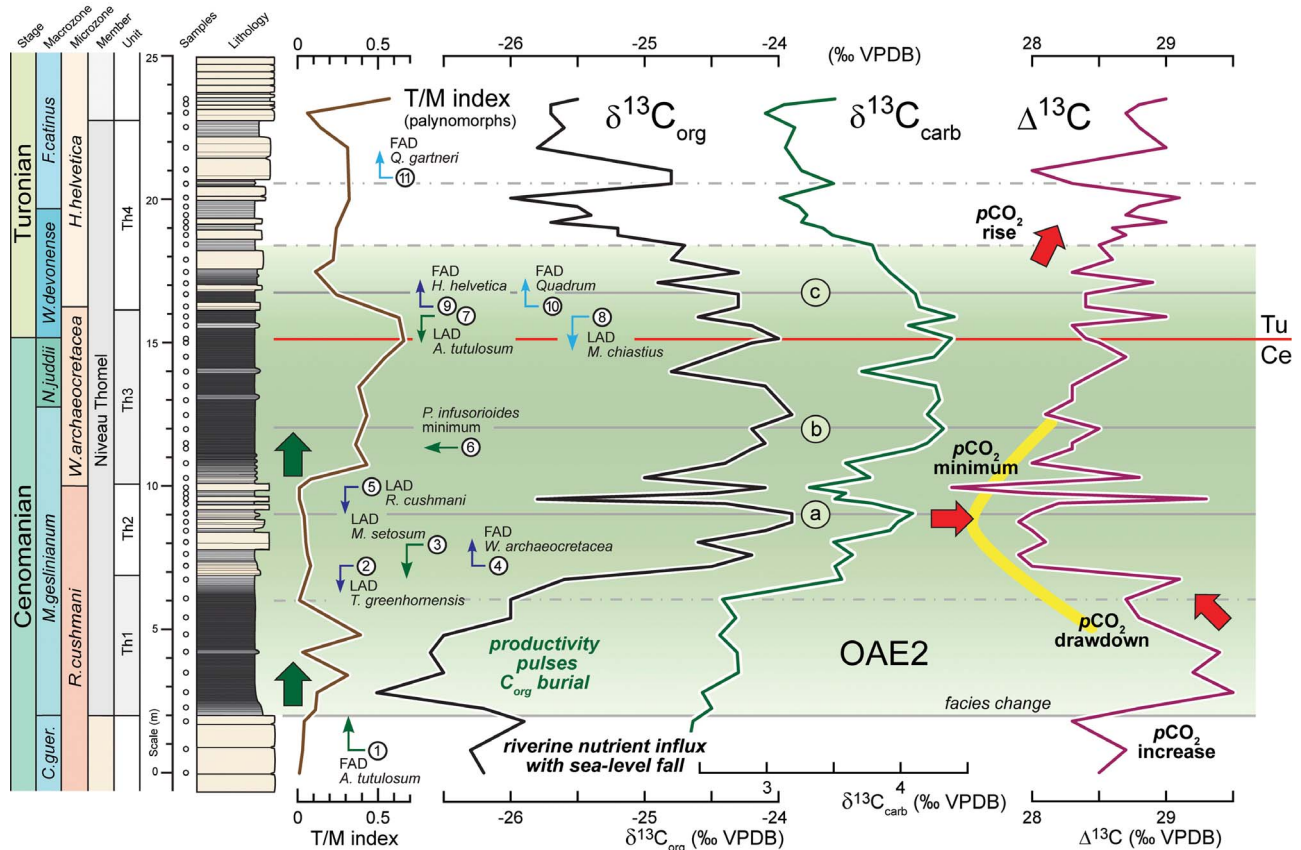


Figure 5. Interpreted carbon-isotope stratigraphy of the CTB at Pont d'Issole. T/M index is proportion of terrestrial to marine palynomorphs (see text for details).

et al., 1990; Takashima et al., 2009; Fernando et al., 2010]. Rock-Eval pyrolysis of kerogen from the black shales at Pont d'Issole yields an average Hydrogen Index (HI) of 362 mg hydrocarbon/g TOC, an Oxygen Index (OI) of 27 mg CO₂/g TOC and a T_{max} of 420°C [Crumière, 1991], demonstrating that the organic matter is predominantly of marine origin (partially modified by bacteria; Type II) and is immature. The highest TOC (>1%) and HI values (>200 mg HC/g TOC) characterize laminated black shales intervals; both values fall significantly in bioturbated facies, with progressive alteration of organic matter by syngedimentary oxidation indicated by high OI values.

[27] Black shales contain largely (75–90%) sapropelic amorphous organic matter, with subsidiary opaque material (5–15%) and relatively small numbers of recognizable fossil palynomorphs (5–10%). Limestones and gray marls contain little or no amorphous material. Dinocysts generally dominate the palynomorph assemblage, with an average T/M index of 0.22, although bisaccate pollen and trilete spores constitute up to 66% (T/M = 0.66) of the assemblage at the top of the upper black shales (Unit Th3) around the CTB (Figure 5). Increased T/M values in both black shale units, relative to immediately adjacent limestone-marl intervals, indicate periods of increased supply and/or increased preservation of terrestrial organic matter accompanying largely marine organic-matter production.

5.2. Carbon Isotopes

[28] The well-preserved nature of the organic matter with moderate to high TOC values throughout the CTB interval at Pont d'Issole enabled the carbon-isotope composition of the organic fraction to be determined in all samples. The resulting $\delta^{13}C_{org}$ curve is very similar in shape to that for $\delta^{13}C_{carb}$ (Figure 5), but has higher amplitude peaks and has low values of between –24‰ and –27‰; $\delta^{13}C_{carb}$ and $\delta^{13}C_{org}$ display a strong positive correlation (Figures 3d and 5).

[29] Differences between the two carbon-isotope trends may be illustrated by plotting the difference between the paired isotope determinations, expressed as $\Delta^{13}C$ (‰ VPDB). The resulting curve (Figure 5) displays a marked increase at the base of the Niveau Thomel, then falling values to a broad minimum in the middle of the limestone-marl interbeds of Unit Th2, coincident with peak “a” of the CTB carbon isotope excursion, and then rising values above. The $\delta^{13}C_{org}$ and $\Delta^{13}C$ profiles display no similarities to T/M index trends (Figure 5), despite the high proportion (>50%) of terrestrial palynomorphs in the uppermost Cenomanian; $\delta^{13}C_{org}$ values do not rise with increasing T/M index, as would be expected from the isotopically heavier nature of Late Cretaceous terrestrial organic matter at ~–24‰ [Gröcke, 2002; Hasegawa et al., 2003]. This is attributed to the overwhelming dominance of sapropelic amorphous marine organic matter throughout the black shale intervals.

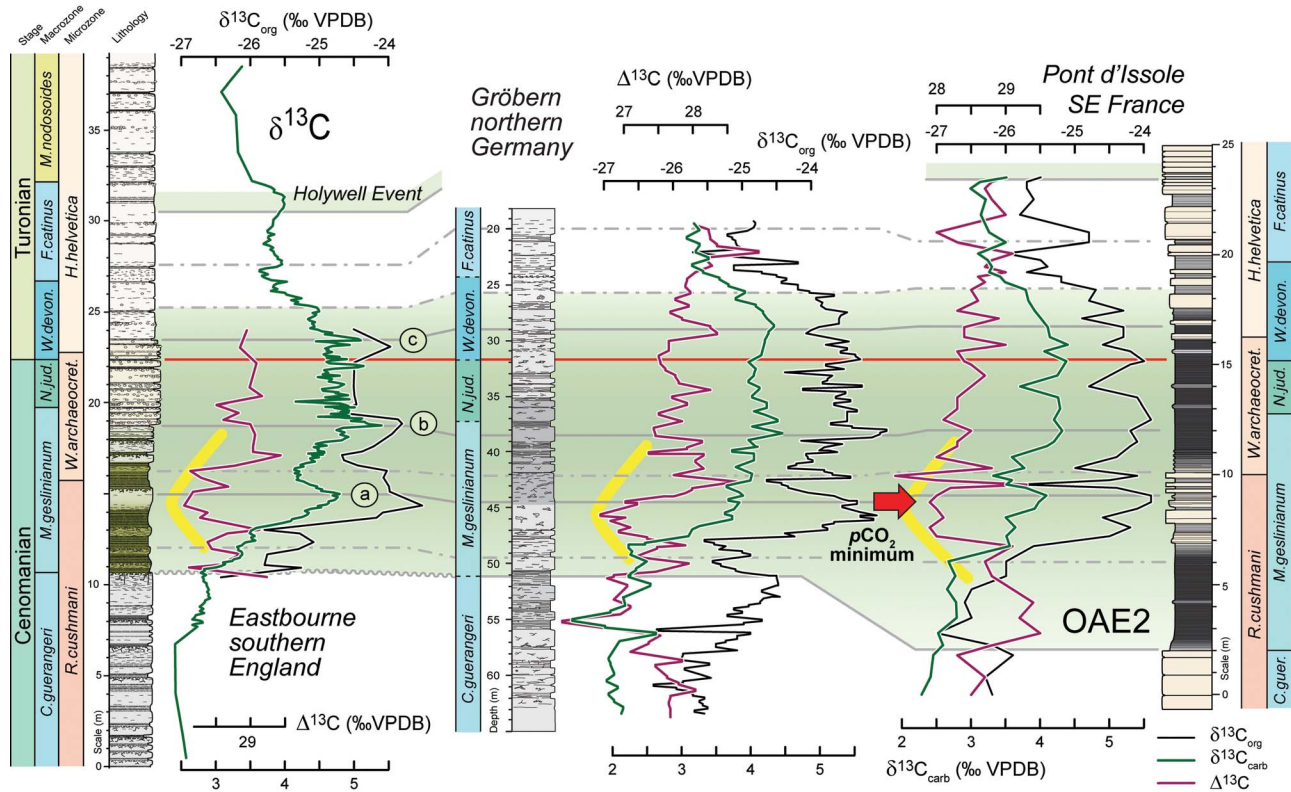


Figure 6. Carbon-isotope correlation between England, Germany, and France. Yellow curve indicates the position of the long-term $\Delta^{13}\text{C}$ minimum developed in all three sections. Eastbourne data are from Paul *et al.* [1999] and Gale *et al.* [2005], Gröbern data are from Voigt *et al.* [2006], and Pont d'Issole data are from this study.

[30] Paired carbonate and organic matter $\delta^{13}\text{C}$ records have been reported from other CTB sections [e.g., Freeman and Hayes, 1992; Tsikos *et al.*, 2004; Sageman *et al.*, 2006; Voigt *et al.*, 2006, 2007; Scopelliti *et al.*, 2008]. However, in many cases, the reliability of one of the data sets is questionable due to (1) an absence of carbonate in the most organic-rich layers and/or insufficient organic matter in some limestones (e.g., the Bonarelli Level at Bottaccione); (2) the occurrence of erratic highly negative values in $\delta^{13}\text{C}_{\text{carb}}$ profiles, indicative of locally precipitated organic-matter-derived carbonate cements (e.g., Tarfaya); and (3) uniform low $\delta^{13}\text{C}_{\text{carb}}$ values, suggesting pervasive overprinting by recrystallization or the addition of extensive homogenous calcite cement (e.g., Bonarelli equivalent, Novara di Sicilia).

[31] Paired carbon isotopes and $\Delta^{13}\text{C}$ curves for three European CTB sections that display no anomalous $\delta^{13}\text{C}_{\text{carb}}$ or $\delta^{13}\text{C}_{\text{org}}$ values, from Eastbourne, Gröbern (Germany) and Pont d'Issole, are shown in Figure 6. The three sections may be correlated at a bed-by-bed scale using a combination of biostratigraphy and chemostratigraphy [Voigt *et al.*, 2006, 2008; this study].

6. Proxies of $p\text{CO}_2$

[32] The large amount of organic matter within the Niveau Thomel and its equivalents worldwide during OAE2, deposited in less than 500 kyr [Voigt *et al.*, 2008], removed substantial amounts of reduced carbon from the surface

carbon cycle. A resulting drawdown of atmospheric CO₂ would be predicted [Arthur *et al.*, 1988], which may be tested using potential $p\text{CO}_2$ proxies. There is increasing evidence of a $p\text{CO}_2$ decrease during OAE2 [Freeman and Hayes, 1992; Kuypers *et al.*, 1999; Barclay *et al.*, 2010; Sinninghe Damsté *et al.*, 2010], but the amount, exact timing, and rate of change remain controversial.

6.1. Carbon Isotopes as a $p\text{CO}_2$ Proxy

[33] Photosynthetic carbon fractionation (ϵ_p) by marine phytoplankton increases with ocean conditions that promote high CO₂ availability in surface waters, such as elevated atmospheric CO₂ concentrations [Dean *et al.*, 1986]. This reaction explains why Cretaceous marine organic matter typically has $\delta^{13}\text{C}$ values that are up to 5–7‰ more negative than its modern equivalent [Arthur *et al.*, 1985a]. It has been proposed that the larger amplitude of the CTB $\delta^{13}\text{C}_{\text{org}}$ excursion (as much as 4–6‰) compared to the $\delta^{13}\text{C}_{\text{carb}}$ excursion (typically ~2‰) in sections worldwide may be attributed to reduced isotopic fractionation between dissolved inorganic carbon and marine organic matter as a consequence of lower atmospheric carbon dioxide (CO₂ drawdown) and increased marine productivity during OAE2 [Arthur *et al.*, 1988; Freeman and Hayes, 1992; Kuypers *et al.*, 1999, 2002; Tsikos *et al.*, 2004; Sinninghe Damsté *et al.*, 2008].

[34] Regional differences in the degree of carbon-isotope fractionation in coeval marine organic matter may be caused by varying rates of productivity. Southern proto-North Atlantic CTB sites, for example, display 2‰ greater amplitude $\delta^{13}\text{C}_{\text{org}}$ excursions than sections elsewhere [Arthur et al., 1988; Sinninghe Damsté et al., 2008]. This difference has been interpreted as being due to higher rates of local CO₂ uptake in surface waters accompanying enhanced primary production, driven by shallowing of the chemocline and increased nutrient input into the photic zone [Laws et al., 1995; Kuypers et al., 2002]. The stable carbon-isotope composition of bulk organic matter will also be affected by changes in the terrestrial contribution to TOC [Kuypers et al., 2004]: Cretaceous marine organic matter typically has $\delta^{13}\text{C}$ ranging from -26‰ to -28‰, and is isotopically lighter than coeval land plant or terrestrial organic C, with average $\delta^{13}\text{C}$ values of -23‰ to -24‰ [Dean et al., 1986; Gröcke, 2002; Hasegawa et al., 2003]. Changes in the degree of preservation of isotopically enriched components of marine organic matter, such as carbohydrate carbon, may also play a role [Sinninghe Damsté and Köster, 1998; Forster et al., 2008].

[35] Stratigraphic variation in the offset between the $\delta^{13}\text{C}_{\text{carb}}$ and $\delta^{13}\text{C}_{\text{org}}$ curves, expressed by $\Delta^{13}\text{C}$, offers a potential tool for tracing paleo- $p\text{CO}_2$ change [cf. Kump and Arthur, 1999], assuming (1) no significant diagenetic alteration of the carbonate or organic carbon $\delta^{13}\text{C}$ values, or a uniform systematic overprinting of these; (2) an overwhelmingly marine or terrestrial organic matter fraction, or a constant proportion of these; and (3) limited temporally restricted productivity effects.

[36] Simplistically, the $\Delta^{13}\text{C}$ curve at Pont d'Issole (Figure 5) may be interpreted to show (1) a marked increase in $p\text{CO}_2$ in the Upper Cenomanian basal *Metoicoceras geslinianum* zone at the onset of black shale deposition, with maximum $p\text{CO}_2$ for the CTB succession in the lower part of the basal black shale; (2) a sharply falling $p\text{CO}_2$ trend for ~80 kyr (timescale of Voigt et al. [2008]) from 1 m above the base of the black shale, indicating the operation of the oceans as a net carbon sink following the onset of organic carbon deposition; (3) a broadly defined $p\text{CO}_2$ minimum in the uppermost Cenomanian at the summit of Th2, coincident with peak "a" of the $\delta^{13}\text{C}$ profiles, and the temporary cessation of black shale deposition, and immediately preceding the extinction of *Rotalipora*; and (4) erratic but gradually rising $p\text{CO}_2$ through the remainder of the CTB succession, despite renewed black shale sedimentation, but with $p\text{CO}_2$ values in the earliest Turonian not attaining peak Cenomanian values.

[37] Comparison between Pont d'Issole and $\Delta^{13}\text{C}$ records from sections at Eastbourne and Gröbern that lack black shales shows excellent agreement between the shapes of the three curves and their interpreted $p\text{CO}_2$ records (Figure 6). The sections may be correlated at high-resolution using a combination of biostratigraphy and $\delta^{13}\text{C}$ chemostratigraphy. Arguably, not only the long-term trends, but also the finer detail of the $\Delta^{13}\text{C}$ curve at Pont d'Issole is seen in the high-resolution Gröbern data. These records are from different facies, located in different sedimentary basins in contrasting paleogeographic settings (Figure 1b), and have different diagenetic histories. Their high similarity offers strong

support for the argument that $\Delta^{13}\text{C}$ provides a robust $p\text{CO}_2$ proxy record.

[38] At both Eastbourne and Gröbern, $\Delta^{13}\text{C}$ values fall by 1.2‰ at the level of the inferred $p\text{CO}_2$ drawdown event, while at Pont d'Issole they fall by 1.6‰. The greater amplitude change at Pont d'Issole is consistent with a higher rate of local CO₂ uptake in surface waters due to greater surface water productivity accompanying black shale deposition in the northern Tethys. The reliability of $\Delta^{13}\text{C}$ as a $p\text{CO}_2$ proxy for the CTB interval may be tested by comparison to independent $p\text{CO}_2$ proxies from corresponding successions elsewhere.

6.2. Biomarker $p\text{CO}_2$ Proxies

[39] Sinninghe Damsté et al. [2008] studied the $\delta^{13}\text{C}$ compositions of individual biomarkers in CTB black shales representing the lower part of OAE2 in the Cape Verde Basin (Figure 1a) of the equatorial proto-North Atlantic (DSDP Site 367). The $\delta^{13}\text{C}$ values of S-bound phytane and C₃₅ hopane were used to calculate $p\text{CO}_2$ levels. Pre-OAE values were estimated at 1300–1400 ppmv falling to 680–980 ppmv $p\text{CO}_2$ coincident with peak "a" of the CTB carbon-isotope excursion [cf. Forster et al., 2007, Figure 4; Sinninghe Damsté et al., 2008, Figure 3], a ~25% drop. These values are somewhat lower than previous biomarker-based $p\text{CO}_2$ estimates [Freeman and Hayes, 1992; Kuypers et al., 1999; Bice et al., 2006], indicating a drawdown that could have reached 40–80%, albeit with very large uncertainties. Nonetheless, the trends and stratigraphic position of the $p\text{CO}_2$ minimum correspond exactly with our interpretation based on European $\Delta^{13}\text{C}$ records (Figure 6).

6.3. Terrestrial $p\text{CO}_2$ Paleoproxy Record

[40] Barclay et al. [2010] presented a quantitative $p\text{CO}_2$ terrestrial proxy record from the CTB interval based on a composite section for the U.S. Western Interior Seaway (WIS; Figure 1a). An estimated 26% decrease in $p\text{CO}_2$ was documented during the Late Cenomanian, based on stomata counts in fossil leaf material (stomatal index method) from WIS sediments. Rapidly rising $p\text{CO}_2$ occurred from 500 kyr before the $\delta^{13}\text{C}$ excursion, reaching a maximum at the beginning of *Sciponoceras gracile* ammonite zone (= base *M. geslinianum* zone equivalent) time, and then with falling values toward the end of the zone (Figure 7). No data were available for the uppermost Cenomanian and Lower Turonian, although low $p\text{CO}_2$ values were reported from the lowest Middle Turonian. Two pronounced short-term $p\text{CO}_2$ minima occur on the longer term trend: one coincident with a small $\delta^{13}\text{C}_{\text{org}}$ peak immediately below the base of the *S. gracile* zone, the other coincident with $\delta^{13}\text{C}_{\text{org}}$ peak "a" in the middle of the zone.

[41] The WIS composite section of Barclay et al. [2010] and its associated $p\text{CO}_2$ record are correlated to Pont d'Issole in Figure 7. The stomatal index method is characterized by a large asymmetric 95% confidence envelope, particularly at high $p\text{CO}_2$, so calculated values vary by up to a factor of three. Late Cenomanian $p\text{CO}_2$ background values are estimated at 300–470 ppmv (average 370 ppmv), rising by as much as 600 ppmv to 320–900 ppmv (average 500 ppmv) within the lower OAE2 interval. The fall from the $p\text{CO}_2$ maximum in the basal *S. gracile* zone reaches a

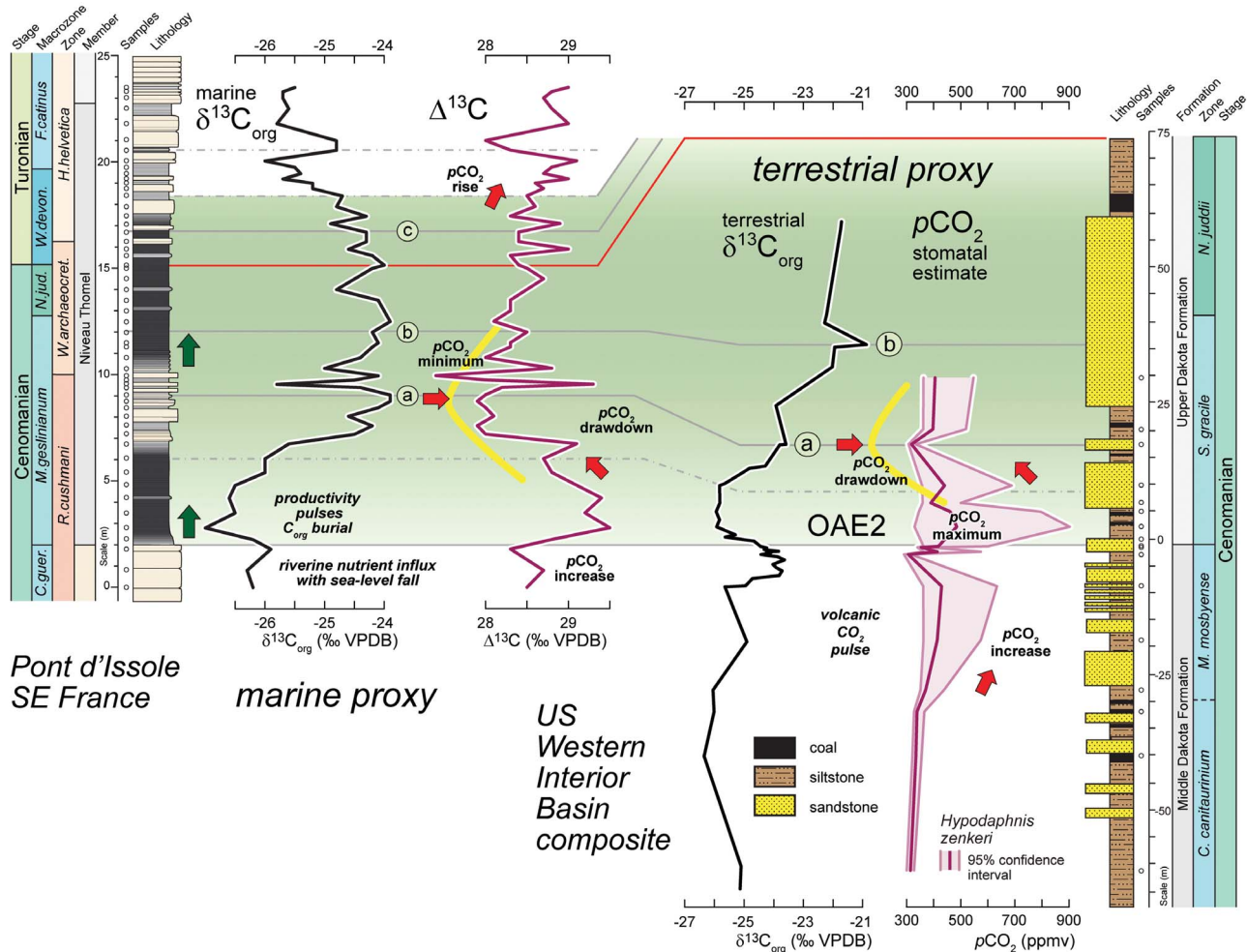


Figure 7. Comparison of the marine $\delta^{13}\text{C}_{\text{org}}$ and $\Delta^{13}\text{C}$ paleo- $p\text{CO}_2$ proxy records at Pont d'Issole with the terrestrial $\delta^{13}\text{C}_{\text{org}}$ and $p\text{CO}_2$ record of *Barclay et al.* [2010], based on stomata counts in fossil leaves from the U.S. Western Interior Seaway (WIS). The terrestrial-based $p\text{CO}_2$ curve based on *Hypodaphnis zenkeri* leaves has been calibrated using a transfer function approach; the colored envelope indicates 95% confidence intervals. Correlation of the sections is based on carbon-isotope stratigraphy and biostratigraphy, incorporating data from multiple WIS sections [Barclay et al., 2010]. The bottom and top of the *Sciponoceras gracile* ammonite zone, equivalent to the *Metoicoceras geslinianum* zone in Europe (Figure 5), provide biostratigraphic datum levels that are consistent with the $\delta^{13}\text{C}$ correlation: a and b are $\delta^{13}\text{C}$ maxima.

minimum of 320 ppmv in the middle of the zone, before rising again above.

6.4. Change of $p\text{CO}_2$ During OAE2

[42] The terrestrial leaf stomata-based $p\text{CO}_2$ record is remarkably similar to the marine $\Delta^{13}\text{C}$ curve (Figure 7), and provides strong support for the hypothesis that the latter offers a good proxy for $p\text{CO}_2$ change. Trends are also consistent with the marine biomarker proxy data from Atlantic black shales [Sinninghe Damsté et al., 2008], even though the $p\text{CO}_2$ values derived by this method are approximately double those calculated using the stomatal index approach. Nonetheless, the relative amount of drawdown is in good agreement, estimated to be ~25%.

[43] Given the uncertainties in the data and a lack of quantitative paleoenvironmental constraints (e.g., dissolved

phosphate concentration of surface waters), the preserved CTB $\Delta^{13}\text{C}$ values in the European sections are not considered to be suitable to calculate reliable absolute $p\text{CO}_2$ concentrations [e.g., Kump and Arthur, 1999, equation 10]. Nonetheless, $\Delta^{13}\text{C}$ offers potential for generating biostratigraphically well-constrained high-resolution time series because it does not require abnormal organic matter preservation (i.e., well-preserved fossil leaf material or marine biomarkers). In the case of all three $p\text{CO}_2$ proxies: $\Delta^{13}\text{C}$; marine biomarker $\delta^{13}\text{C}$; and leaf stomata data; the precise correlation of the $p\text{CO}_2$ drawdown events with positive $\delta^{13}\text{C}_{\text{org}}$ excursions, particularly OAE2 peak “a,” is consistent with increased preservation and burial of organic matter during OAE2 having modulated and temporarily reversed a trend of rising atmospheric CO_2 through the Late Cenomanian.

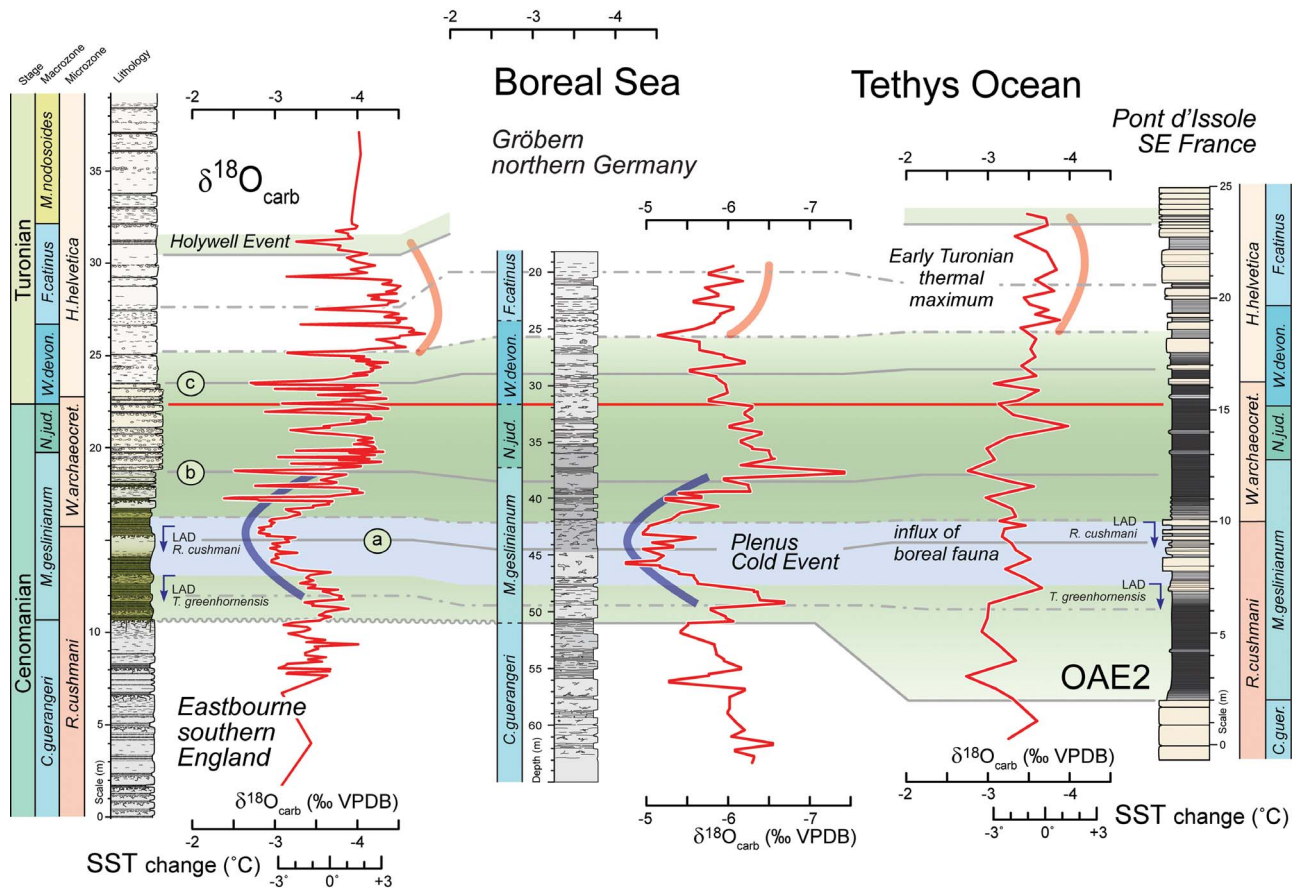


Figure 8. Oxygen stable-isotope profiles for Boreal and Tethyan sites. Tie lines are based on biostratigraphic and carbon-isotope correlation (Figure 6). Blue curve and horizontal blue band indicate the extent of the sea surface temperature (SST) minimum ($\delta^{18}\text{O}$ maximum) corresponding to the Plenus Cold Event. Pale red curve shows the position of the Early Turonian thermal maximum. Note the greater amplitude of the paleoclimate signal in the Boreal sites. Eastbourne $\delta^{18}\text{O}$ data are from Paul *et al.* [1999], Gröbern data are from Voigt *et al.* [2006], and Pont d'Issole data are from this study. Relative changes in SST calculated using the paleotemperature equation of Anderson and Arthur [1983] assuming a value of -1‰ $\delta^{18}\text{O}_w$ VSMOW for Late Cretaceous seawater.

[44] A pulse of increased silicate weathering causing $p\text{CO}_2$ drawdown during a period of accelerated hydrological cycling, which is indicated by a short-term transitory increase in radiogenic strontium (a $^{87}\text{Sr}/^{86}\text{Sr}$ peak) at the onset of OAE2 in some CTB sections, may also have occurred [Frijia and Parente, 2008; Jenkyns, 2010].

7. Sea Surface Temperature Change

[45] Atmospheric CO_2 concentrations are arguably the primary driver of SST variation over geological timescales [Royer *et al.*, 2004; Fletcher *et al.*, 2008]. In the light of the $p\text{CO}_2$ proxy records presented above, generally rising SST would be predicted to accompany rising $p\text{CO}_2$ during the Late Cenomanian, with temporary cooling during the mid-*M. geslinianum* zone and other $p\text{CO}_2$ drawdown events. This supposition may be tested using oxygen stable-isotope and TEX_{86} biomarker data.

7.1. Oxygen Isotope Records

[46] Secular trends in the oxygen stable-isotope composition of bulk pelagic carbonate have been proposed to provide a proxy for changes in average SST [Jenkyns *et al.*, 1994; Clarke and Jenkyns, 1999]. Good agreement between $\delta^{18}\text{O}$ trends derived from bulk sediments and their enclosed pristine planktic foraminifera, support this proposal [e.g., Voigt *et al.*, 2010].

[47] Falling bulk sediment $\delta^{18}\text{O}$ values through the Upper Cenomanian, with a minimum in the lowest Turonian, at the summit of the Niveau Thomel, occur at Pont d'Issole (Figure 8) and are also seen in longer term oxygen-isotope records from elsewhere in the Vocontian Basin at Vergons and Lambuisse [Lignum, 2009; Takashima *et al.*, 2009]. Similar Cretaceous $\delta^{18}\text{O}$ minima in the Lower Turonian, interpreted to represent a period of maximum global SSTs during an Early Turonian climatic optimum, are recorded in northern Europe [Jenkyns *et al.*, 1994] and in the Southern Hemisphere [Clarke and Jenkyns, 1999]; $\delta^{18}\text{O}$ data for

individual planktic foraminifera species from low-latitude western Atlantic sites support this interpretation [Huber et al., 2002; Forster et al., 2007; Friedrich et al., 2008].

[48] The $\delta^{18}\text{O}$ record at Pont d'Issole is compared with those at Eastbourne and Gröbern in Figure 8. The correlation lines in Figure 8 are based on $\delta^{13}\text{C}$ chemostratigraphy constrained by biostratigraphy, with no account taken of the $\delta^{18}\text{O}$ profiles. Isotope values at Pont d'Issole and Eastbourne are similar at around -3 to -4‰ $\delta^{18}\text{O}$, while those at Gröbern are 2 – 3‰ lighter, likely reflecting the formerly deeper burial of the Elbe Valley Graben section (Figure 1b). Nonetheless, the two northern European sites show very similar $\delta^{18}\text{O}$ profiles with greater variation than at Pont d'Issole, the most obvious features being high SST (low $\delta^{18}\text{O}$) at the beginning of OAE2, followed by distinct cooling (increasing $\delta^{18}\text{O}$) through the lower *M. geslinianum* zone, a minimum in the middle of the zone at the extinction point of *Rotalipora*, and then sharply rising SST (falling $\delta^{18}\text{O}$) through the upper part of the zone.

[49] Using $\delta^{18}\text{O}$ values from the less diagenetically altered Eastbourne section, and the paleotemperature equation of Anderson and Arthur [1983] assuming an average value of -1‰ $\delta^{18}\text{O}_w$ VSMOW for Late Cretaceous seawater [Shackleton and Kennett, 1975], the relative SST fall during early *M. geslinianum* time was $\sim 4^\circ\text{C}$ (Figure 8). A smaller $\delta^{18}\text{O}$ maximum occurs in both sections immediately below the base of the *M. geslinianum* zone, representing $\sim 2^\circ\text{C}$ of SST cooling. Applying the orbital time scale of Voigt et al. [2008], the *M. geslinianum* zone cooling occurred in ~ 40 kyr and, overall, the cold episode (Plenus Cold Event; blue band in Figure 8) lasted < 60 kyr, before the onset of further warming. A seawater temperature rise during late *M. geslinianum* zone time of $> 4^\circ\text{C}$ indicated by the Eastbourne $\delta^{18}\text{O}$ curve (Figure 8) is confirmed by $\delta^{18}\text{O}$ data for pristine brachiopod shells from northern European chalks [Voigt et al., 2004, 2006].

[50] The paleotemperature interpretation from Eastbourne might be regarded as an oversimplification because the isotopic composition of surface waters varies with latitude due to changes in precipitation minus evaporation. Taking a 38°N paleolatitude for Eastbourne and applying the latitude correction of Zachos et al. [1994] yields a local surface water value of -0.6‰ $\delta^{18}\text{O}_w$. Applying this to the paleotemperature equation increases estimated paleotemperatures by around 2°C . However, it has no effect on the temperature range of values reported. It is acknowledged that absolute SST values derived from bulk chalk $\delta^{18}\text{O}$ are likely to be overestimates due to diagenesis [Pearce et al., 2009]. However, it is believed that as a consequence of a uniform overprint toward lighter values, relative changes in isotopic composition caused by changing SST are largely preserved.

[51] The Late Cenomanian midlatitude SST cooling events identified above correspond exactly with $p\text{CO}_2$ minima interpreted from $\Delta^{13}\text{C}$ for the three European CTB sections and leaf stomatal index data from the WIS. Furthermore, the relative amplitude of the two CO₂ drawdown events, with the lower having approximately half the amplitude of the upper event, is reflected in all three data sets: $\Delta^{13}\text{C}$ values; stomatal $p\text{CO}_2$ estimates; and $\delta^{18}\text{O}$ SST.

[52] There is no clear coincident shift to higher $\delta^{18}\text{O}$ values reflecting cooler SST at the top of the *R. cushmani* zone at Pont d'Issole (Figure 8). Absence of this shift may

be due to the lesser temperature sensitivity of the lower latitude Tethyan marginal basin site to global $p\text{CO}_2$ change, and/or diagenetic differences between the black shale (Th1, Th3) intervals and the intervening interbedded marls and limestones (Th2) masking short-term $\delta^{18}\text{O}$ trends. The SST paleotemperature interpretation presented here may be tested using an independent SST proxy, namely the TEX₈₆ organic paleothermometer.

7.2. TEX₈₆ Organic Paleothermometry

[53] The organic paleothermometer TEX₈₆ (tetraether index of 86 carbon atoms) [Schouten et al., 2002], based on the relative distribution of glycerol dialkyl glycerol tetraether (GDGT) membrane lipids specific for marine Crenarchaeota picoplankton, is being used increasingly to reconstruct SSTs from ancient organic-rich sediments. The TEX₈₆ proxy utilizes an empirically observed positive correlation between annual mean SST and variations in the composition of specific GDGTs. Several different temperature calibrations have been proposed for TEX₈₆ [Kim et al., 2008, 2010; Liu et al., 2009] that produce very different SST values in the $> 30^\circ\text{C}$ range (e.g., Figure 9). However, these differences are systematic and do not significantly affect relative paleotemperature trends.

[54] Attempts to obtain a TEX₈₆ record from Pont d'Issole proved unsuccessful. Out of five black shale samples examined, only one yielded GDGTs and at far too low concentrations to use for paleotemperature determination (E. C. van Bentum, personal communication, 2009). However, work on selected North Atlantic CTB black shales has demonstrated high TEX₈₆ values of up to 0.96 [Schouten et al., 2003]. Three ocean drilling sites (Figure 1a): ODP Site 1260 (Demerara Rise, offshore Suriname) and DSDP Site 367 (Cape Verde Basin, offshore Senegal) in the equatorial proto-North Atlantic [Forster et al., 2007]; and ODP Site 1276 (Newfoundland Basin, offshore Canada) in the midlatitude proto-North Atlantic [Sinninghe Damsté et al., 2010], have provided $\delta^{13}\text{C}_{\text{org}}$ profiles coupled with TEX₈₆-based paleo-SST records for CTB boundary black shale successions.

[55] The highest resolution TEX₈₆-based paleo-SST record of the CTB interval is from ODP Site 1276 [Sinninghe Damsté et al., 2010]; the midlatitude position of this Newfoundland Basin site is similar to that of the European sections discussed here. Estimated TEX₈₆-based SSTs across the boundary interval are extremely high at 33° – 42°C and are punctuated by a large cooling event ($> 5^\circ\text{C}$) down to 29° – 31°C , coincident with peak “a” of the carbon-isotope excursion (Figure 9). Rising SSTs above peak “a” at ODP Site 1276 are punctuated by a second, less pronounced cooling phase of 2° – 5°C before the reestablishment of more stable warm conditions in the later part of OAE2. Based on carbon-isotope stratigraphy, the main cooling event was synchronous with $\sim 4^\circ\text{C}$ cooling in TEX₈₆-based SST records from equatorial Atlantic sites [Forster et al., 2007], although the later smaller cooling event is less evident in the lower amplitude, lower resolution records from these sites.

[56] Comparison between equatorial and the midlatitude TEX₈₆ records shows that at the start of OAE2 there was no significant difference in SST in the tropics and at 30°N , while during peak cooling a 3° – 6°C difference developed [Sinninghe Damsté et al., 2010]. This indicates a significantly

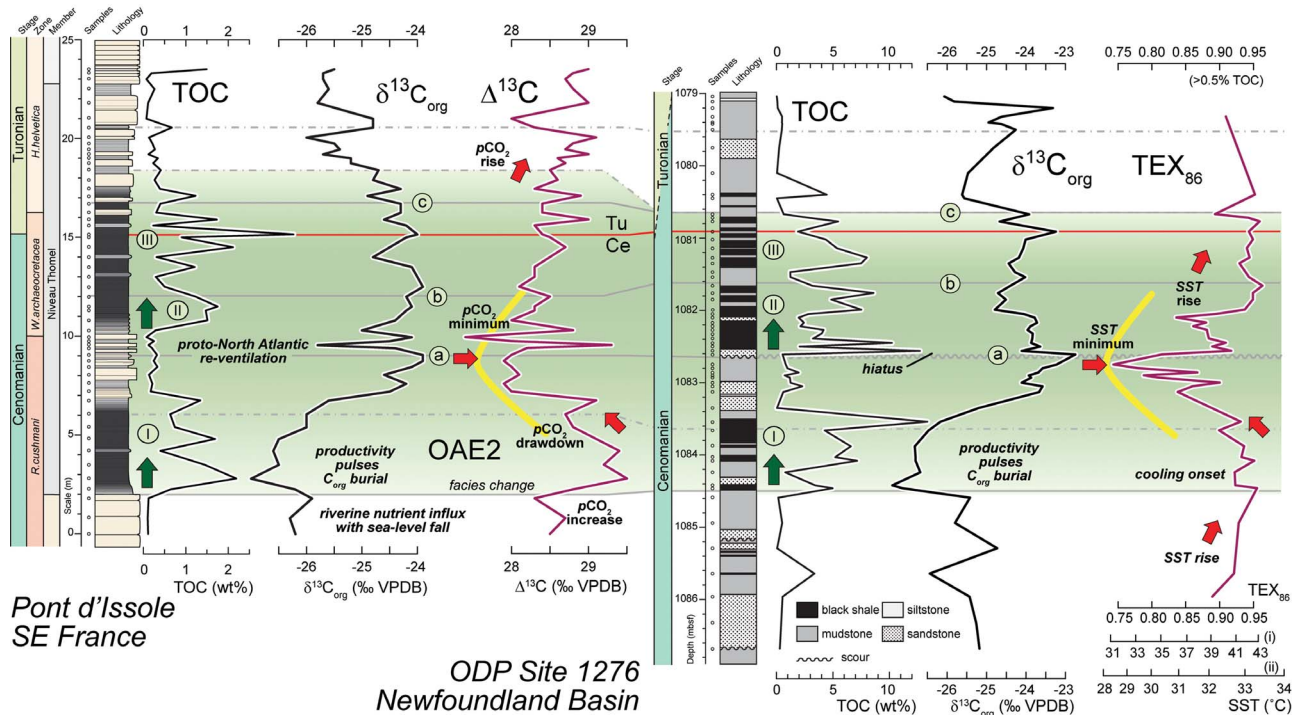


Figure 9. Correlation of the $\Delta^{13}\text{C}$ paleo- $p\text{CO}_2$ proxy record at Pont d'Issole with the TEX_{86} paleo-sea surface temperature (SST, °C) record from ODP Site 1276, Newfoundland Basin. Total organic carbon and $\delta^{13}\text{C}_{\text{org}}$ records are shown for comparison: Pont d'Issole data are from this study, Site 1276 data are from *Sinninghe Damsté et al.* [2010]. TEX_{86} temperature scales based on (1) linear [Kim et al., 2008] and (2) reciprocal [Liu et al., 2009] calibrations with SST. Site 1276 lithology and stratigraphy reinterpreted from *Shipboard Scientific Party* [2004]; correlation of the Cenomanian-Turonian boundary (red horizontal line) is based on the $\delta^{13}\text{C}_{\text{org}}$ curves.

increased latitudinal thermal gradient accompanying $p\text{CO}_2$ drawdown, and suggests strong coupling between atmospheric CO_2 and latitudinal thermal gradients in the mid-Cretaceous greenhouse world.

8. Faunal Records and Biotic Turnover

[57] A widespread SST cooling event during the early stages of OAE2 might be expected to impact the Cenomanian biota. The presence of a North Boreal “pulse” fauna including the belemnite *Praeactinocamax plenus* (Blainville), the bivalve *Oxytoma seminudum* (Dames), and the serpulid worm *Hamulus* sp. in uppermost Plenus Marl Bed 3 to Bed 6 at Eastbourne, and throughout southern England and northern France [Jefferies, 1962], indicates the temporary southward spread of cooler northern surface waters during the Late Cenomanian. The stratigraphic range of this pulse fauna corresponds closely with the temporary shift to high $\delta^{18}\text{O}$ values at Eastbourne and Gröbern reflecting SST cooling (Figure 8). The occurrence of *P. plenus*, *O. seminudum* and *Hamulus* sp. at an equivalent level in glauconitic marl facies at Les Lattes [Gale and Christensen, 1996], 35 km SE of Pont d'Issole, and a general influx of Boreal species into the Tethyan region [Kuhnt et al., 1986] further demonstrate the widespread nature of the linked paleoclimatic and faunal event. This phenom-

on has been termed the “Plenus Cold Event” [Gale and Christensen, 1996].

[58] The LAD of the large keeled planktonic foraminifera *Rotalipora* occurs immediately below the base of the upper black shales at Pont d'Issole (top of Unit Th2, Figure 4). It has been proposed that the extinction of rotaliporids was caused by widespread intensification and expansion of oxygen-minimum zones which compromised the process of gametogenesis in deep-dwelling keeled planktonic foraminifera [Jarvis et al., 1988]. However, rotaliporids occur consistently, albeit in small numbers, throughout the lower black shale successions at both Pont d'Issole [Groszheny et al., 2006] and Lambruisse [Takashima et al., 2009] and are common in the overlying limestones of Th2, so their extinction does not match the onset of regional black shale deposition and likely bottom water anoxia. Therefore, it is more likely that, as proposed by Pearce et al. [2009], the extinction of *Rotalipora* was triggered by climate cooling and water mass reorganization accompanying the Plenus Cold Event, rather than water column anoxia.

9. Linking Organic Carbon Burial, $p\text{CO}_2$, and SST

[59] The appearance of black shales in the CTB intervals at both Pont d'Issole and in the Newfoundland Basin at ODP Site 1276 is followed by rising $\delta^{13}\text{C}$ values that attain

a maximum at the summit of the *R. cushmani* zone, defining peak “a” of the OAE2 carbon-isotope stratigraphy (Figure 9). Data from multiple onshore and offshore sections show that $p\text{CO}_2$ drawdown accompanied the onset of major black shale deposition and was followed by a period of temporary SST cooling that reached a maximum during a $p\text{CO}_2$ minimum. It has even been suggested that $p\text{CO}_2$ dropped sufficiently low to initiate a floral change from C₃- to C₄-plant-dominated vegetation in NW Africa at this time [Kuypers *et al.*, 1999].

[60] TOC contents at both Pont d’Issole and ODP Site 1276 decrease in the interval of the $p\text{CO}_2$ and SST minima that are coincident with carbon isotope peak “a,” with uppermost *R. cushmani* zone and equivalent beds being devoid of black shale, prior to the onset of later black shale deposition. The sharp coincident breaks in the TOC, $\delta^{13}\text{C}_{\text{org}}$ and TEX₈₆ profiles immediately above “a” at ODP Site 1276 indicate a significant hiatus at the base of the upper black shale succession at that site. However, the temporary disappearance of black shales in CTB sections is not unusual: at Wunstorf, northern Germany, the interval between carbon-isotope peaks “a” and “b” corresponds to the only short eccentricity cycle within the CTB interval that is free of black shales [Voigt *et al.*, 2008].

[61] Synchronous with the Plenus Cold Event, a period of extensive bottom water reoxidation occurred throughout the Atlantic region, as indicated by the recolonization of previously anoxic seafloors (areas of black shale deposition) by benthic foraminifera off South America (Demerara Rise [Friedrich *et al.*, 2006; van Bentum *et al.*, 2009]), North Africa (Morocco [Keller and Pardo, 2004]) and in North America [Leckie *et al.*, 1998]. This relationship suggests that SST cooling led to enhanced water mass mixing that transferred oxygen and heat from surface to deep waters. Cooling SST and falling $p\text{CO}_2$ would have been accompanied by rising $p\text{O}_2$, further driving increased marine oxygenation. Reoxygenation may explain the temporary facies change to low-TOC sediments with increased bioturbation that is coincident with the $\Delta^{13}\text{C}$ minimum (e.g., Unit Th2 of the Niveau Thomel at Pont d’Issole). However, recycling of nutrients into the photic zone would have refueled primary production in continental-margin areas, and led to the return of anoxia, including periods of local photic-zone euxinia [Sinninghe Damsté and Köster, 1998; Kuypers *et al.*, 2002; Jenkyns *et al.*, 2007], and renewed black shale accumulation (peak OAE2) during the latest Cenomanian.

[62] Renewed increases in $p\text{CO}_2$, SST and $\delta^{13}\text{C}$ during latest Cenomanian black shale deposition suggest that a continuing volcanogenic CO₂ flux overrode further drawdown effects. Degassing accompanying the initial emplacement of the Caribbean large igneous plateau (LIP) between 95.1 and 92.2 Ma [Sinton and Duncan, 1997; Snow *et al.*, 2005; Kuroda *et al.*, 2007] provides the likely CO₂ source; a massive short-lived hydrothermal pulse at the onset of OAE2 is evidenced by marine osmium-isotope records [Turgeon and Creaser, 2008]. The temporary nature of CO₂ drawdown during OAE2 reflects the delicate balance between global organic carbon burial and weathering rates versus the CO₂ input flux, none of which are well constrained.

[63] The termination of OAE2 during a period of continuing rises in $p\text{CO}_2$ and SST points to other factors causing the cessation of widespread organic matter deposition in the oceans. One factor might be that flooding of continental interiors accompanying the latest Cenomanian transgression and early Turonian eustatic highstand resulted in lower rates of erosion (higher base level), reduced weathering, a falling terrestrial nutrient supply, and more efficient sequestration of nutrients by nearshore sediments, with a resulting fall in open-ocean productivity.

10. Conclusion

[64] Stratigraphic variation in $\Delta^{13}\text{C}$ through the CTB interval overwhelmingly reflects a positive correlation between the degree of carbon-isotope fractionation by marine phytoplankton and $p\text{CO}_2$ concentration, and therefore offers a good $p\text{CO}_2$ proxy. $\Delta^{13}\text{C}$ trends show excellent agreement with complementary $p\text{CO}_2$ proxy records based on marine biomarker $\delta^{13}\text{C}$ and fossil leaf stomata counts.

[65] The $p\text{CO}_2$ increased rapidly during the Late Cenomanian, with a major CO₂ pulse ~20 kyr prior to the onset of major organic carbon burial. This is attributed to elevated rates of volcanic degassing accompanying high seafloor spreading rates combined with a massive magmatic pulse, attributed to intense volcanic activity accompanying the initial emplacement of the Caribbean large igneous plateau.

[66] A sharp reversal to falling $p\text{CO}_2$ began shortly after the onset of black shale deposition in midlatitudes and an episode of enhanced burial of organic matter in the equatorial proto-North Atlantic at ~93.95 Ma. This represented a phase of negative feedback in the short term carbon cycle due to increased carbon burial, likely enhanced by increased silicate weathering.

[67] A pronounced broad $p\text{CO}_2$ minimum occurred ~93.86 Ma. The amount of $p\text{CO}_2$ decrease is estimated at 25% of Late Cenomanian values, based on multiple proxy data. A further $p\text{CO}_2$ rise, beginning in the $\delta^{13}\text{C}$ trough interval and continuing through and beyond the later phases of black shale deposition, indicates continued input of volcanic greenhouse gas emissions and reduced negative feedback during the later phases of OAE2.

[68] Significant short-term sea surface temperature (SST) variation during OAE2 is indicated by coherent temperature proxy records. Stratigraphic relationships indicate that $p\text{CO}_2$ variation during CTB times acted as a first-order driver on SST, with generally rising Late Cenomanian SSTs punctuated by an episode of >4°C cooling at midlatitudes accompanying CO₂ drawdown. Substantially increased latitudinal temperature gradients at this time likely led to increased ocean mixing rates, improved deepwater ventilation in the proto-North Atlantic, and the temporary cessation of black shale deposition at midlatitudes. Rapid SST warming of >4°C accompanied rising $\delta^{13}\text{C}$ and transgression in the second build-up phase of the CTB carbon isotope event. An Early Turonian thermal maximum followed the termination of OAE2. This study confirms $p\text{CO}_2$ variation caused by changing volcanic gas emissions combined with negative feedback from organic matter deposition during OAE2, as a major driver of Cenomanian-Turonian SSTs and by inference, global climate change.

[69] **Acknowledgments.** Danièle Grosheny provided detailed field logs of Pont d'Issole. Kevin Attree and Joanne Peterkin assisted in the generation of the organic-carbon isotope data. Brad Sageman and an anonymous referee are thanked for their constructive reviews. J.L. acknowledges receipt of a Kingston University research studentship and support from Statoil Norway (project 4500867860). D.R.G. and I.J. acknowledge funding by U.K. Natural Environment Research Council (NERC) grants NE/H020756/1 and NE/H021868/1.

References

- Adams, D. D., M. T. Hurtgen, and B. B. Sageman (2010), Volcanic triggering of a biogeochemical cascade during Oceanic Anoxic Event 2, *Nat. Geosci.*, **3**, 201–204, doi:10.1038/ngeo743.
- Anderson, T. F., and M. A. Arthur (1983), Stable isotopes of oxygen and carbon and their application to sedimentologic and paleoenvironmental problems, in *Stable Isotopes in Sedimentary Geology*, edited by M. A. Arthur et al., *SEPM Short Course*, **10**, 1–151.
- Arthur, M. A., W. E. Dean, and G. E. Claypool (1985a), Anomalous ¹³C enrichment in modern marine organic carbon, *Nature*, **315**, 216–218, doi:10.1038/315216a0.
- Arthur, M. A., W. E. Dean, and S. O. Schlanger (1985b), Variations in the global carbon cycle during the Cretaceous related to climate, volcanism and changes in atmospheric CO₂, in *The Carbon Cycle and Atmospheric CO₂: Natural Variations Archean to Present*, *Geophys. Monogr. Ser.*, vol. 32, edited by E. T. Sundquist and W. S. Broecker, pp. 504–529, AGU, Washington, D. C.
- Arthur, M. A., S. O. Schlanger, and H. C. Jenkyns (1987), The Cenomanian/Turonian Oceanic Anoxic Event, II: Palaeoceanographic controls on organic matter production and preservation, in *Marine Petroleum Source Rocks*, edited by J. Brooks and A. J. Fleet, *Geol. Soc. London Spec. Publ.*, **26**, 401–420.
- Arthur, M. A., W. E. Dean, and L. M. Pratt (1988), Geochemical and climatic effects of increased marine organic carbon burial at the Cenomanian/Turonian boundary, *Nature*, **335**, 714–717, doi:10.1038/335714a0.
- Barclay, R. S., J. C. McElwain, and B. B. Sageman (2010), Carbon sequestration activated by a volcanic CO₂ pulse during Ocean Anoxic Event 2, *Nat. Geosci.*, **3**, 205–208, doi:10.1038/ngeo757.
- Barron, E. J. (1983), A warm, equable Cretaceous: The nature of the problem, *Earth Sci. Rev.*, **19**, 305–338, doi:10.1016/0012-8252(83)90001-6.
- Berner, R. A. (2006), GEOCARBSULF: A combined model for Phanerozoic atmospheric O₂ and CO₂, *Geochim. Cosmochim. Acta*, **70**, 5653–5664, doi:10.1016/j.gca.2005.11.032.
- Bice, K. L., D. Birgel, P. A. Meyers, K. A. Dahl, K. U. Hinrichs, and R. D. Norris (2006), A multiple proxy and model study of Cretaceous upper ocean temperatures and atmospheric CO₂ concentrations, *Paleoceanography*, **21**, PA2002, doi:10.1029/2005PA001203.
- Clarke, L. J., and H. C. Jenkyns (1999), New oxygen isotope evidence for long-term Cretaceous climatic change in the Southern Hemisphere, *Geology*, **27**, 699–702, doi:10.1130/0091-7613(1999)027<0699: NOIEFL>2.3.CO;2.
- Crumière, J. P. (1989), Crise anoxique à la limite Cénomanien-Turonien dans le bassin subalpin oriental (sud-est de la France). Relation avec l'eustatisme, *Geobios Mem. Spec.*, **22**, suppl. 1, 189–203, doi:10.1016/S0016-6995(89)80056-7.
- Crumière, J. P. (1991), Les potentialités pétrolières des dépôts du Bassin Vocontien oriental (sud-est France) au Cenomanien-Turonien inférieur. Dynamiques de la sédimentation, de la préservation et de l'évolution de la matière organique, Ph.D. thesis, 78 pp, Univ. Claude-Bernard Lyon I, Lyon, France.
- Crumière, J. P., C. Crumière-Airaud, J. Espitalié, and P. Cotillon (1990), Global and regional controls on potential source-rock deposition and preservation: The Cenomanian-Turonian Oceanic Anoxic Event (CTOAE) on the European Tethyan margin (southeastern France), in *Deposition of Organic Facies*, edited by A. Y. Huc, *AAPG Stud. Geol.*, **30**, 107–118.
- Dean, W. E., M. A. Arthur, and G. E. Claypool (1986), Depletion of ¹³C in Cretaceous marine organic matter: Source, diagenetic or environmental signal?, *Mar. Geol.*, **70**, 119–157, doi:10.1016/0025-3227(86)90092-7.
- Fernando, A. G. S., R. Takashima, H. Nishi, F. Giraud, and H. Okada (2010), Calcareous nannofossil biostratigraphy of the Thomel Level (OAE2) in the Lambruisse section, Vocontian Basin, southeast France, *Geobios*, **43**, 45–57, doi:10.1016/j.geobios.2009.11.003.
- Fletcher, B. J., S. J. Brentnall, C. W. Anderson, R. A. Berner, and D. J. Beerling (2008), Atmospheric carbon dioxide linked with Mesozoic and early Cenozoic climate change, *Nat. Geosci.*, **1**, 43–48, doi:10.1038/ngeo.2007.29.
- Forster, A., S. Schouten, K. Moriya, P. A. Wilson, and J. S. Sinninghe Damsté (2007), Tropical warming and intermittent cooling during the Cenomanian/Turonian oceanic anoxic event 2: Sea surface temperature records from the equatorial Atlantic, *Paleoceanography*, **22**, PA1219, doi:10.1029/2006PA001349.
- Forster, A., M. M. M. Kuypers, S. C. Turgeon, H. J. Brumsack, M. R. Petrizzo, and J. S. Sinninghe Damsté (2008), The Cenomanian/Turonian oceanic anoxic event in the South Atlantic: New insights from a geochemical study of DSDP Site 530A, *Palaeogeogr. Palaeoclimatol. Palaeoecol.*, **267**, 256–283, doi:10.1016/j.palaeo.2008.07.006.
- Freeman, K. H., and J. M. Hayes (1992), Fractionation of carbon isotopes by phytoplankton and estimates of ancient CO₂ levels, *Global Biogeochem. Cycles*, **6**, 185–198, doi:10.1029/92GB00190.
- Friedrich, O., J. Erbacher, and J. Mutterose (2006), Paleoenvironmental changes across the Cenomanian/Turonian Boundary Event (Oceanic Anoxic Event 2) as indicated by benthic foraminifera from the Demerara Rise (ODP Leg 207), *Rev. Micropaleontol.*, **49**, 121–139, doi:10.1016/j.revmic.2006.04.003.
- Friedrich, O., J. Erbacher, K. Moriya, P. A. Wilson, and H. Kuhnert (2008), Warm saline intermediate waters in the Cretaceous tropical Atlantic Ocean, *Nat. Geosci.*, **1**, 453–457, doi:10.1038/ngeo217.
- Frijia, G., and M. Parente (2008), Strontium isotope stratigraphy in the upper Cenomanian shallow-water carbonates of the southern Apennines: Short-term perturbations of marine ⁸⁷Sr/⁸⁶Sr during the oceanic anoxic event 2, *Palaeogeogr. Palaeoclimatol. Palaeoecol.*, **261**, 15–29, doi:10.1016/j.palaeo.2008.01.003.
- Gale, A. S., and W. G. Christensen (1996), Occurrence of the belemnite *Actinocamax plenus* in the Cenomanian of SE France and its significance, *Bull. Geol. Soc. Den.*, **43**, 68–77.
- Gale, A. S., W. J. Kennedy, S. Voigt, and I. Walaszczyk (2005), Stratigraphy of the Upper Cenomanian–Lower Turonian Chalk succession at Eastbourne, Sussex, UK: Ammonites, inoceramid bivalves and stable carbon isotopes, *Cretaceous Res.*, **26**, 460–487, doi:10.1016/j.cretres.2005.01.006.
- Gröcke, D. R. (2002), The carbon isotope composition of ancient CO₂ based on higher-plant organic matter, *Philos. Trans. R. Soc. London, Ser. A*, **360**, 633–658, doi:10.1098/rsta.2001.0965.
- Grosheny, D., B. Beaudoin, L. Morel, and D. Desmares (2006), High-resolution biostratigraphy and chemostratigraphy of the Cenomanian/Turonian boundary event in the Vocontian Basin, southeast France, *Cretaceous Res.*, **27**, 629–640, doi:10.1016/j.cretres.2006.03.005.
- Hasegawa, T. (1997), Cenomanian–Turonian carbon isotope events recorded in terrestrial organic matter from northern Japan, *Palaeogeogr. Palaeoclimatol. Palaeoecol.*, **130**, 251–273, doi:10.1016/S0031-0182(96)00129-0.
- Hasegawa, T., L. M. Pratt, H. Maeda, Y. Shigeta, T. Okamoto, T. Kase, and K. Uemura (2003), Upper Cretaceous stable carbon isotope stratigraphy of terrestrial organic matter from Sakhalin, Russian Far East: A proxy for the isotopic composition of paleoatmospheric CO₂, *Palaeogeogr. Palaeoclimatol. Palaeoecol.*, **189**, 97–115, doi:10.1016/S0031-0182(02)00634-X.
- Huber, B. T., D. A. Hodell, and C. P. Hamilton (1995), Middle–Late Cretaceous climate of the southern high-latitudes: Stable isotopic evidence for minimal equator-to-pole thermal gradients, *Geol. Soc. Am. Bull.*, **107**, 1164–1191, doi:10.1130/0016-7606(1995)107<1164: MLCCOT>2.3.CO;2.
- Huber, B. T., R. D. Norris, and K. G. MacLeod (2002), Deep-sea paleotemperature record of extreme warmth during the Cretaceous, *Geology*, **30**, 123–126, doi:10.1130/0091-7613(2002)030<0123:DSPROE>2.0.CO;2.
- Jarvis, I. (2003), Sample preparation in ICP-MS, in *Handbook of Inductively Coupled Plasma Mass Spectrometry*, edited by K. E. Jarvis, A. L. Gray, and R. S. Houk, pp. 172–224, Viridian, Woking, U. K.
- Jarvis, I., G. A. Carson, M. K. E. Cooper, M. B. Hart, P. N. Leary, B. A. Tocher, D. Horne, and A. Rosenfeld (1988), Microfossil assemblages and the Cenomanian–Turonian (late Cretaceous) oceanic anoxic event, *Cretaceous Res.*, **9**, 3–103, doi:10.1016/0195-6671(88)90003-1.
- Jarvis, I., A. S. Gale, H. C. Jenkyns, and M. A. Pearce (2006), Secular variation in Late Cretaceous carbon isotopes and sea-level change: Evidence from a new ^δ¹³C carbonate reference curve for the Cenomanian–Campanian (99.6–70.6 Ma), *Geol. Mag.*, **143**, 561–608, doi:10.1017/S0016756806002421.
- Jefferies, R. P. S. (1962), The palaeoecology of the *Actinocamax plenus* subzone (lowest Turonian) in the Anglo-Paris Basin, *Palaentology*, **4**, 609–647.
- Jenkyns, H. C. (2010), Geochemistry of oceanic anoxic events, *Geochem. Geophys. Geosyst.*, **11**, Q03004, doi:10.1029/2009GC002788.
- Jenkyns, H. C., A. S. Gale, and R. M. Corfield (1994), Carbon- and oxygen-isotope stratigraphy of the English Chalk and Italian Scaglia and its palaeoclimatic significance, *Geol. Mag.*, **131**, 1–34, doi:10.1017/S0016756800010451.

- Jenkyns, H. C., A. Matthews, H. Tsikos, and Y. Erel (2007), Nitrate reduction, sulfate reduction, and sedimentary iron isotope evolution during the Cenomanian–Turonian oceanic anoxic event, *Paleoceanography*, *22*, PA3208, doi:10.1029/2006PA001355.
- Keller, G., and A. Pardo (2004), Age and paleoenvironment of the Cenomanian–Turonian global stratotype section and point at Pueblo, Colorado, *Mar. Micropaleontol.*, *51*, 95–128, doi:10.1016/j.marmicro.2003.08.004.
- Kim, J. H., S. Schouten, E. C. Hopmans, B. Donner, and J. S. Sinninghe Damsté (2008), Global sediment core-top calibration of the TEX₈₆ paleothermometer in the ocean, *Geochim. Cosmochim. Acta*, *72*, 1154–1173, doi:10.1016/j.gca.2007.12.010.
- Kim, J.-H., J. van der Meer, S. Schouten, P. Helmke, V. Willmott, F. Sangiorgi, N. Koç, E. C. Hopmans, and J. S. Sinninghe Damsté (2010), New indices and calibrations derived from the distribution of crenarchaeal isoprenoid tetraether lipids: Implications for past sea surface temperature reconstructions, *Geochim. Cosmochim. Acta*, *74*, 4639–4654, doi:10.1016/j.gca.2010.05.027.
- Kuhnt, W., J. Thurow, J. Wiedmann, and J. P. Herbin (1986), Oceanic anoxic conditions around the Cenomanian/Turonian boundary and the response of the biota, in *Biogeochemistry of Black Shales*, *Mitt. Geol. Palaontol. Inst. Univ. Hamburg*, vol. 60, edited by E. T. Degens, P. A. Meyers, and S. C. Brassell, pp. 205–246, Geol. Palaontol. Inst. Univ. Hamburg, Hamburg, Germany.
- Kump, L. R., and M. A. Arthur (1999), Interpreting carbon-isotope excursions: Carbonates and organic matter, *Chem. Geol.*, *161*, 181–198, doi:10.1016/S0009-2541(99)00086-8.
- Kuroda, J., N. O. Ogawa, M. Tanimizu, M. F. Coffin, H. Tokuyama, H. Kitazato, and N. Ohkouchi (2007), Contemporaneous massive subaerial volcanism and late Cretaceous Oceanic Anoxic Event 2, *Earth Planet. Sci. Lett.*, *256*, 211–223, doi:10.1016/j.epsl.2007.01.027.
- Kuypers, M. M. M., R. D. Pancost, and J. S. Sinninghe Damsté (1999), A large and abrupt fall in atmospheric CO₂ concentration during Cretaceous times, *Nature*, *399*, 342–345, doi:10.1038/20659.
- Kuypers, M. M. M., R. D. Pancost, I. A. Nijenhuis, and J. S. Sinninghe Damsté (2002), Enhanced productivity led to increased organic carbon burial in the euxinic North Atlantic basin during the late Cenomanian oceanic anoxic event, *Paleoceanography*, *17*(4), 1051, doi:10.1029/2000PA000569.
- Kuypers, M. M. M., L. J. Lourens, W. R. C. Rijpstra, R. D. Pancost, I. A. Nijenhuis, and J. S. Sinninghe Damsté (2004), Orbital forcing of organic carbon burial in the proto-North Atlantic during oceanic anoxic event 2, *Earth Planet. Sci. Lett.*, *228*, 465–482, doi:10.1016/j.epsl.2004.09.037.
- Larson, R. L. (1991), Geological consequences of superplumes, *Geology*, *19*, 963–966, doi:10.1130/0091-7613(1991)019<0963:GCOS>2.3.CO;2.
- Laws, E. A., B. N. Popp, R. R. Bidigare, M. C. Kennicutt, and S. A. Macko (1995), Dependence of phytoplankton carbon isotope composition on growth rate and (CO₂)_{aq}: Theoretical considerations and experimental results, *Geochim. Cosmochim. Acta*, *59*, 1131–1138, doi:10.1016/0016-7037(95)00030-4.
- Leckie, R. M., R. F. Yuretich, O. L. O. West, D. Finkelstein, and M. Schmidt (1998), Paleocyanography of the southwestern Western Interior Sea during the time of the Cenomanian–Turonian boundary, Late Cretaceous, in *Stratigraphy and Paleoenvironments of the Cretaceous Western Interior Seaway, USA*, edited by W. E. Dean and M. A. Arthur, *SEPM Concepts Sedimentol. Paleontol.*, *6*, 101–126.
- Lignum, J. (2009), Cenomanian (Upper Cretaceous) palynology and chemostratigraphy: Dinoflagellate cysts as indicators of paleoenvironmental and sea-level change, Ph.D. thesis, 582 pp., Kingston Univ. London, Kingston upon Thames, U. K.
- Lignum, J., I. Jarvis, and M. A. Pearce (2008), A critical assessment of standard processing methods for the preparation of palynological samples, *Rev. Palaeobot. Palynol.*, *149*, 133–149, doi:10.1016/j.revpalbo.2007.11.004.
- Liu, Z. H., M. Pagani, D. Zinniker, R. DeConto, M. Huber, H. Brinkhuis, S. R. Shah, R. M. Leckie, and A. Pearson (2009), Global cooling during the Eocene–Oligocene climate transition, *Science*, *323*, 1187–1190, doi:10.1126/science.1166368.
- Meyer, K. M., and L. R. Kump (2008), Oceanic euxinia in Earth history: Causes and consequences, *Annu. Rev. Earth Planet. Sci.*, *36*, 251–288, doi:10.1146/annurev.earth.36.031207.124256.
- Morel, L. (1998), Stratigraphie à haute résolution du passage Cénomaniens–Turonien, Ph.D. thesis, 224 pp., Univ. de Paris VI Pierre et Marie Curie, Paris.
- Mort, H. P., T. Adatte, K. B. Follmi, G. Keller, P. Steinmann, V. Matera, Z. Berner, and D. Stuben (2007), Phosphorus and the roles of productivity and nutrient recycling during oceanic anoxic event 2, *Geology*, *35*, 483–486, doi:10.1130/G23475A.1.
- Ogg, J. G., G. Ogg, and F. M. Gradstein (2008), *The Concise Geologic Time Scale*, 177 pp., Cambridge Univ. Press, Cambridge, U. K.
- Paul, C. R. C., M. A. Lamolda, S. F. Mitchell, M. R. Vaziri, A. Gorostidi, and J. D. Marshall (1999), The Cenomanian–Turonian boundary at Eastbourne (Sussex, UK): A proposed European reference section, *Paleoogeogr. Palaeoclimatol. Palaeoecol.*, *150*, 83–121, doi:10.1016/S0031-0182(99)00009-7.
- Pearce, M. A., I. Jarvis, and B. A. Tocher (2009), The Cenomanian–Turonian boundary event, OAE2 and paleoenvironmental change in epicontinental seas: New insights from the dinocyst and geochemical records, *Paleoogeogr. Palaeoclimatol. Palaeoecol.*, *280*, 207–234, doi:10.1016/j.palaeo.2009.06.012.
- Philip, J., et al. (2000), Map 14: Late Cenomanian, in *Atlas Peri-Tethys Palaeogeographical Maps*, edited by J. Dercourt et al., Comm. de la Carte Geol. du Monde, Paris.
- Pross, J. (2001), Paleo-oxygenation in Tertiary epeiric seas: Evidence from dinoflagellate cysts, *Paleoogeogr. Palaeoclimatol. Palaeoecol.*, *166*, 369–381, doi:10.1016/S0031-0182(00)00219-4.
- Royer, D. L., R. A. Berner, I. P. Montañez, N. J. Tabor, and D. J. Beerling (2004), CO₂ as a primary driver of Phanerozoic climate, *GSA Today*, *14*, 4–10, doi:10.1130/1052-5173(2004)014<4:CAAPDO>2.0.CO;2.
- Sageman, B. B., S. R. Meyers, and M. A. Arthur (2006), Orbital time scale and new C-isotope record for Cenomanian–Turonian boundary stratotype, *Geology*, *34*, 125–128, doi:10.1130/G22074.1.
- Schlanger, S. O., and H. C. Jenkyns (1976), Cretaceous oceanic anoxic events: Causes and consequences, *Geol. Mijnbouw*, *55*, 179–184.
- Schlanger, S. O., M. A. Arthur, H. C. Jenkyns, and P. A. Scholle (1987), The Cenomanian–Turonian Oceanic Anoxic event, I. Stratigraphy and distribution of organic carbon-rich beds and the marine δ¹³C excursion, in *Marine Petroleum Source Rocks*, edited by J. Brooks and A. J. Fleet, *Geol. Soc. London Spec. Publ.*, *26*, 371–399.
- Scholle, P. A., and M. A. Arthur (1980), Carbon isotope fluctuation in Cretaceous pelagic limestones: Potential stratigraphic and petroleum exploration tool, *AAPG Bull.*, *64*, 67–87.
- Schouten, S., E. C. Hopmans, E. Schefuss, and J. S. Sinninghe Damsté (2002), Distributional variations in marine crenarchaeal membrane lipids: A new tool for reconstructing ancient sea water temperatures?, *Earth Planet. Sci. Lett.*, *204*, 265–274, doi:10.1016/S0012-821X(02)00979-2.
- Schouten, S., E. C. Hopmans, A. Forster, Y. van Breugel, M. M. M. Kuypers, and J. S. Sinninghe Damsté (2003), Extremely high sea-surface temperatures at low latitudes during the middle Cretaceous as revealed by archaeal membrane lipids, *Geology*, *31*, 1069–1072, doi:10.1130/G19876.1.
- Scopelliti, G., A. Bellanca, E. Erba, H. C. Jenkyns, R. Neri, P. Tamagnini, V. Luciani, and D. Masetti (2008), Cenomanian–Turonian carbonate and organic-carbon isotope records, biostratigraphy and provenance of a key section in NE Sicily, Italy: Palaeoceanographic and palaeogeographic implications, *Paleoogeogr. Palaeoclimatol. Palaeoecol.*, *265*, 59–77, doi:10.1016/j.palaeo.2008.04.022.
- Seton, M., C. Gaina, R. D. Muller, and C. Heine (2009), Mid-Cretaceous seafloor spreading pulse: Fact or fiction?, *Geology*, *37*, 687–690, doi:10.1130/G25624A.1.
- Shackleton, N. J., and J. P. Kennett (1975), Paleotemperature history of the Cenozoic and the initiation of Antarctic glaciation: Oxygen and carbon isotope analyses in DSDP sites 277, 279, and 281, edited by J. P. Kennett et al., *Initial Rep. Deep Sea Drill. Proj.*, *29*, 743–755.
- Shipboard Scientific Party (2004), Site 1276, in *Drilling the Newfoundland Half of the Newfoundland–Iberia Transect: The First Conjugate Margin Drilling in a Nonvolcanic Rift Sites 1276 and 1277*, edited by B. E. Tucholke, J.-C. Sibuet, and A. Klaus, *Proc. Ocean Drill. Program Initial Rep.*, *210*, doi:10.2973/odp.proc.ir.210.103.2004.
- Sinninghe Damsté, J. S., and J. Köster (1998), A euxinic southern North Atlantic Ocean during the Cenomanian/Turonian oceanic anoxic event, *Earth Planet. Sci. Lett.*, *158*, 165–173, doi:10.1016/S0012-821X(98)00052-1.
- Sinninghe Damsté, J. S., M. M. M. Kuypers, R. D. Pancost, and S. Schouten (2008), The carbon isotopic response of algae, (cyano)bacteria, archaea and higher plants to the late Cenomanian perturbation of the global carbon cycle: Insights from biomarkers in black shales from the Cape Verde Basin (DSDP Site 367), *Org. Geochem.*, *39*, 1703–1718, doi:10.1016/j.orggeochem.2008.01.012.
- Sinninghe Damsté, J. S., E. C. van Bentum, G. J. Reichart, J. Pross, and S. Schouten (2010), A CO₂ decrease-driven cooling and increased latitudinal temperature gradient during the mid-Cretaceous Oceanic Anoxic Event 2, *Earth Planet. Sci. Lett.*, *293*, 97–103, doi:10.1016/j.epsl.2010.02.027.
- Sinton, C. W., and R. A. Duncan (1997), Potential links between ocean plateau volcanism and global ocean anoxia at the Cenomanian–Turonian boundary, *Econ. Geol.*, *92*, 836–842, doi:10.2113/gsecongeo.92.7-8.836.
- Snow, L. J., R. A. Duncan, and T. J. Bralower (2005), Trace element abundances in the Rock Canyon Anticline, Pueblo, Colorado, marine sedimentary section and their relationship to Caribbean plateau construction and oxygen anoxic event 2, *Paleoceanography*, *20*, PA3005, doi:10.1029/2004PA001093.

- Takashima, R., H. Nishi, K. Hayashi, H. Okada, H. Kawahata, T. Yamanaka, A. G. Fernando, and M. Mampuku (2009), Litho-, bio- and chemostratigraphy across the Cenomanian/Turonian boundary (OAE 2) in the Vocontian Basin of southeastern France, *Palaeogeogr. Palaeoclimatol. Palaeoecol.*, *273*, 61–74, doi:10.1016/j.palaeo.2008.12.001.
- Tsandeov, I., and C. P. Slomp (2009), Modeling phosphorus cycling and carbon burial during Cretaceous Oceanic Anoxic Events, *Earth Planet. Sci. Lett.*, *286*, 71–79, doi:10.1016/j.epsl.2009.06.016.
- Tsikos, H., et al. (2004), Carbon-isotope stratigraphy recorded by the Cenomanian-Turonian Oceanic Anoxic Event: Correlation and implications based on three key localities, *J. Geol. Soc.*, *161*, 711–719, doi:10.1144/0016-764903-077.
- Turgeon, S. C., and R. A. Creaser (2008), Cretaceous oceanic anoxic event 2 triggered by a massive magmatic episode, *Nature*, *454*, 323–326, doi:10.1038/nature07076.
- van Bentum, E. C., A. Hetzel, H. J. Brumsack, A. Forster, G. J. Reichart, and J. S. Sinninghe Damsté (2009), Reconstruction of water column anoxia in the equatorial Atlantic during the Cenomanian-Turonian oceanic anoxic event using biomarker and trace metal proxies, *Palaeogeogr. Palaeoclimatol. Palaeoecol.*, *280*, 489–498, doi:10.1016/j.palaeo.2009.07.003.
- Voigt, S., A. S. Gale, and S. Flogel (2004), Midlatitude shelf seas in the Cenomanian-Turonian greenhouse world: Temperature evolution and North Atlantic circulation, *Paleoceanography*, *19*, PA4020, doi:10.1029/2004PA001015.
- Voigt, S., A. S. Gale, and T. Voigt (2006), Sea-level change, carbon cycling and palaeoclimate during the Late Cenomanian of northwest Europe; an integrated palaeoenvironmental analysis, *Cretaceous Res.*, *27*, 836–858, doi:10.1016/j.cretres.2006.04.005.
- Voigt, S., A. Aurag, F. Leis, and U. Kaplan (2007), Late Cenomanian to Middle Turonian high-resolution carbon isotope stratigraphy: New data from the Münsterland Cretaceous Basin, Germany, *Earth Planet. Sci. Lett.*, *253*, 196–210, doi:10.1016/j.epsl.2006.10.026.
- Voigt, S., J. Erbacher, J. Mutterlose, W. Weiss, T. Westerhold, F. Wiese, M. Wilmssen, and T. Wonik (2008), The Cenomanian-Turonian of the Wunstorf section (North Germany): Global stratigraphic reference section and new orbital time scale for Oceanic Anoxic Event 2, *Newsl. Stratigr.*, *43*, 65–89, doi:10.1127/0078-0421/2008/0043-0065.
- Voigt, S., O. Friedrich, R. D. Norris, and J. Schönfeld (2010), Campanian-Maastrichtian carbon isotope stratigraphy: Shelf-ocean correlation between the European shelf sea and the tropical Pacific Ocean, *Newsl. Stratigr.*, *44*, 57–72, doi:10.1127/0078-0421/2010/0004.
- Wedepohl, K. H. (1971), Environmental influences on the chemical composition of shales and clays, in *Phys. Chem. Earth*, *8*, 305–333.
- Wilpshaar, M., H. Leereveld, and H. Visscher (1997), Early Cretaceous sedimentary and tectonic development of the Dauphinois Basin (SE France), *Cretaceous Res.*, *18*, 457–468, doi:10.1006/crest.1997.0062.
- Zachos, J. C., L. D. Stott, and K. C. Lohmann (1994), Evolution of early Cenozoic marine temperatures, *Paleoceanography*, *9*, 353–387, doi:10.1029/93PA03266.

D. R. Gröcke, Department of Earth Sciences, Durham University, Science Labs, Durham DH1 3LE, UK.

I. Jarvis, Centre for Earth and Environmental Science Research, School of Geography, Geology and the Environment, Kingston University London, Penrhyn Road, Kingston upon Thames KT1 2EE, UK. (i.jarvis@kingston.ac.uk)

H. C. Jenkyns, Department of Earth Sciences, University of Oxford, South Parks Road, Oxford OX1 3AN, UK.

J. S. Lignum, Ichron Limited, Century House, Gadbrook Business Centre, Northwich, CW9 7TL, UK.

M. A. Pearce, Statoil Gulf Services LLC, 2103 CityWest Blvd., Houston, TX 77042, USA.